Comparison of ^{13}CO Line and Far-Infrared Continuum Emission as a Diagnostic of Dust and Molecular Gas Physical Conditions:
III. Systematic Effects and Scientific Implications

W. F. Wall

Instituto Nacional de Astrofísica, Óptica, y Electrónica, Apdo. Postal 51 y 216, Puebla, Pue., México

`wwall@inaoep.mx`

ABSTRACT

Far-infrared continuum data from the *COBE/DIRBE* instrument were combined with Nagoya 4-m ^{13}CO J $= 1 \rightarrow 0$ spectral line data to infer the multiparsec-scale physical conditions in the Orion A and B molecular clouds, using $140\,\mu$m$/240\,\mu$m dust color temperatures and the $240\,\mu$m$/^{13}$CO J $= 1 \rightarrow 0$ intensity ratios. In theory, the ratio of far-IR, submillimeter, or millimeter continuum to that of a ^{13}CO (or C^{18}O) rotational line can place reliable upper limits on the temperature of the dust and molecular gas on multi-parsec scales; on such scales, both the line and continuum emission are optically thin, resulting in a continuum-to-line ratio that suffers no loss of temperature sensitivity in the high-temperature limit as occurs for ratios of CO rotational lines or ratios of continuum emission in different wavelength bands.

Two-component models fit the Orion data best, where one has a fixed-temperature and the other has a spatially varying temperature. The former represents gas and dust towards the surface of the clouds that are heated primarily by a very large-scale (i.e. $\sim 1\,$kpc) interstellar radiation field. The latter represents gas and dust at greater depths into the clouds and are shielded from this interstellar radiation field and heated by local stars. The inferred physical conditions are consistent with those determined from previously observed maps of ^{12}CO J $= 1 \rightarrow 0$ and J $= 2 \rightarrow 1$ that cover the entire Orion A and B molecular clouds. The models require that the dust-gas temperature difference is $0\pm 2\,$K. If this surprising result applies to much of the Galactic ISM, except in

unusual regions such as the Galactic Center, then there are a number implications. These include dust-gas thermal coupling that is commonly factors of 5 to 10 stronger than previously believed, Galactic-scale molecular gas temperatures closer to $20\,\mathrm{K}$ than to $10\,\mathrm{K}$, an improved explanation for the $N(H_2)/I(CO)$ conversion factor (a full discussion of this is deferred to a later paper), and ruling out at least one dust grain alignment mechanism. The simplest interpretation of the models suggests that about 40–50% of the Orion clouds are in the form of cold (i.e. $\sim$ 3-10 K) dust and gas, although alternative explanations are not ruled out. These alternatives include the contribution to the $240\,\mu\mathrm{m}$ continuum by dust associated with atomic hydrogen and reduced ^{13}CO abundance towards the clouds' edges. Even considering these alternatives, it is still likely that cold material with temperatures of $\sim$ 7-10 K still exists. If this cold gas and dust are common in the Galaxy, then mass estimates of the Galactic ISM must be revised upwards by up to 60%.

The feasibility of submillimeter or millimeter continuum to ^{13}CO line ratios constraining estimates of dust and molecular gas temperatures was tested. The model fits allowed the simulation of the necessary millimeter-continuum and ^{13}CO J $= 1 \rightarrow 0$ maps used in the test. In certain "hot spots" — that have continuum-to-line ratios above some threshold value — the millimeter continuum to ^{13}CO ratio can estimate the dust temperature to within a factor of 2 over large ranges of physical conditions. Nevertheless, supplemental observations of the ^{13}CO J $= 2 \rightarrow 1$ line or of shorter wavelength continuum are advisable in placing lower limits on the estimated temperature. Even without such supplemental observations, this test shows that the continuum-to-line ratio places reliable upper limits on the temperature.

Subject headings: ISM: molecules and dust — Orion

1.   Introduction

While interesting in themselves, molecular clouds provide insights into star formation. Since stars form in and from molecular clouds, knowing the physical conditions within these clouds is essential for a complete understanding of star formation. As mentioned in Paper I (Wall 2007), the warm (i.e., $\gtrsim 50$–$100\,\mathrm{K}$) molecular gas associated with star formation is often identified and diagnosed from observations of different rotational lines of CO (e.g., Wilson et al. 2001; Plume et al. 2000; Howe et al. 1993; Graf et al. 1993, 1990; Boreiko and Betz 1989; Fixsen et al. 1999; Harris et al. 1985; Harrison et al. 1999;

Wall et al. 1991; Güsten et al. 1993; Wild et al. 1992; Harris et al. 1991). Molecular gas, and the interstellar medium in general, can also be observed in the millimeter, submillimeter, and far-IR continuum, which trace the emission of the dust grains associated with interstellar gas. Continuum surveys can probe the structure and excitation of the ISM (see, for example, Dupac et al. 2000; Wall et al. 1996; Bally et al. 1991; Zhang et al. 1989; Werner et al. 1976; Heiles et al. 2000; Reach et al. 1998; Boulanger et al. 1998; Lagache et al. 1998; Goldsmith et al. 1997; Sodroski et al. 1994; Boulanger et al. 1990; Sellgren et al. 1990; Scoville & Good 1989; Sodroski et al. 1989; Leisawitz & Hauser 1988). Estimating physical parameters like temperature, and sometimes density, requires using the ratios of intensities of spectral lines or of the continuum at different wavelengths. Given that each of these ratios is dependent on the ratio of two Planck functions at two different wavelengths, they often lose temperature sensitivity at higher temperatures. While there are methods of addressing this shortcoming, having two tracers of molecular gas with different dependences on the temperature would complement other methods of tracing warm dust or molecular gas. This is especially true if the tracers are optically thin, because low opacity emission is more sensitive to the physical parameters of the bulk of the gas, rather than in just the surface layers.

One such pair of tracers is a rotational line of an isotopologue of CO, such as that of ^{13}CO or C^{18}O, and the submillimeter continuum. Both of these tracers are optically thin on the scales of many parsecs, which are the scales of interest for the current work. Schloerb et al. (1987) and Swartz et al. (1989) showed that the intensity ratio of an optically thin isotopic CO line emission to submillimeter continuum emission can estimate the temperature of gas and dust in molecular clouds. The Schloerb et al. (1987) expression for this ratio goes roughly like T^2 in the high-temperature limit. Accordingly, the I_ν(submm)/I(C^{18}O J = 1 → 0) and I_ν(submm)/I(^{13}CO J = 1 → 0) ratios are actually *more sensitive to temperature as that temperature increases.* This is in stark contrast to ratios of rotational lines of a given isotopologue of CO and to ratios of continuum intensities at different frequencies, which *lose* sensitivity to temperature in the high-temperature limit. The I_ν(submm)/I(^{13}CO) ratio can then serve as the needed diagnostic of high gas/dust temperatures, provided that the shortcomings and complications of these tracers can be overcome or at least mitigated. These complications include variations in the ^{13}CO-to-dust mass ratio, non-molecular phases of the ISM along the line of sight, variations of gas density, variations in dust grain properties, appreciable optical depth variations in the ^{13}CO line used, and others (see the Introduction of Paper I for more details). Such complications are often reduced in the case of observations on multi-parsec scales, because spatial gradients on such scales are generally smaller than the extremes that occur on very small scales. Consequently, testing the reliability of the I_ν(submm)/I(^{13}CO) ratio as high-temperature diagnostic is best carried out with observations of a molecular cloud, or of clouds, on multi-parsec scales.

The Orion A and B molecular clouds were chosen as the clouds for testing the $I_\nu(\text{submm})/I(^{13}\text{CO})$ ratio's diagnostic ability. They have been mapped in the ^{13}CO J $= 1 \rightarrow 0$ line (see, e.g., Nagahama et al. 1998) and in the far-IR by *IRAS* (Bally et al. 1991) and *COBE/DIRBE* (Wall et al. 1996, W96 hereafter). Avoiding the complication of the emission of stochastically heated dust grains requires far-IR observations at wavelengths longer than $100\,\mu\text{m}$ (e.g. Désert et al. 1990, W96). Accordingly, the far-IR observations of *COBE/DIRBE* were used instead of *IRAS* because the former has two bands — $\lambda = 140\,\mu\text{m}$ and $240\,\mu\text{m}$ — longward of $100\,\mu\text{m}$, whereas the latter does not. The Orion A and B clouds were chosen for this study because they have the advantages that they are bright in ^{13}CO J $= 1 \rightarrow 0$ and at far-IR wavelengths, are out of the Galactic plane to avoid confusion with foreground and background emission, are several degrees in size so as to accommodate many *DIRBE* beams, and have the best range of dust temperatures at the *DIRBE* resolution of $0°.7$ (see the Introduction of Paper I and *COBE/DIRBE* Explanatory Supplement 1998, for more details). Therefore, the $I_\nu(240\,\mu\text{m})/I(^{13}\text{CO})$ ratio, hereafter called r_{240}, was plotted against the $140\,\mu\text{m}/240\,\mu\text{m}$ dust color temperature, or T_{dc}, to test the r_{240}'s ability to recover molecular cloud physical conditions. Physical models were applied to these data and physical conditions were inferred in Paper I. The reliability of the model results were tested with simulated data in Paper II (Wall 2007a).

The next section summarizes the model results (i.e. Paper I) and the results of the simulations (i.e. Paper II). Section 3 then discusses general systematic effects that had not been treated previously. Section 4 gives the scientific implications of the results.

2. Review of the Results of the Modelling and of the Simulations

The details of the treatment of the data and of the modeling and its results are found in Paper I. After a subtraction of large-scale emission from the Orion $140\,\mu\text{m}$ and $240\,\mu\text{m}$ maps representing foreground/background emission not associated with the Orion clouds (such subtraction was not necessary and, therefore, not applied to the ^{13}CO J $= 1 \rightarrow 0$ map), one-component and two-component model curves were fitted to the observational data in the r_{240} versus T_{dc} plot. There were two types of one-component models: LTE and LVG (a type of non-LTE model). There were also two types of two-component models (both types being using the LVG code): simple two-component models and two-subsample, two-component models. These models all adopted some form of the following assumption:

The only physical parameters that change from one line of sight to the next are the dust temperature, T_d, and the gas kinetic temperature, T_K, while maintaining a constant difference, $\Delta T \equiv T_d - T_K$. Other physical parameters such as gas density, dust-to-gas mass ratio, dust

mass absorption coefficient, etcetera are assumed to be constant from position to position.
This is referred to as the *basic assumption.* In the case of the one-component, LTE models, this means that the only fitted parameter was ΔT, while the T_d and T_K freely varied from position to position. For the one-component, LVG models, the fitted parameters were ΔT, the ^{13}CO column density per velocity interval, $N(^{13}CO)/\Delta v$, and the molecular hydrogen density, $n(H_2)$, while the T_d and T_K freely varied from position to position. Put very explicitly, the basic assumption applied to the one-component, LVG models means that the ΔT, $N(^{13}CO)/\Delta v$, and $n(H_2)$ were assumed to be spatially unchanging and therefore are the parameters to be determined from the model fits. For the simple two-component models, there was a component 0, representing dust and gas in the surface of the clouds and largely heated by a large-scale interstellar radiation field (ISRF), and a component 1, representing dust and gas deeper into the clouds heated by local stars and a large-scale ISRF attenuated by the surface layers of gas and dust. The physical parameters of component 0 were spatially unchanging and the physical parameters of component 1 were also spatially unchanging, except for T_d and T_K. The component-0 parameters were the dust temperature, T_{d0}, the column density per velocity interval, $\frac{N_{c0}(^{13}CO)}{\Delta v_c}$, the density, n_{c0}, and the filling factor relative to component 1, c_0. The component-1 parameters were $\frac{N_{c1}(^{13}CO)}{\Delta v_c}$ and n_{c1}. (The component-1 dust temperature, T_{d1}, varied so as to generate a curve in the r_{240} versus T_{dc} plot. Component 0, for example, would only generate a single point in this plot if there were no component 1 contributing to the model output.) One more parameter derived from the model fit was the ΔT, which was assumed to be the same for both components. The two-subsample, two-component models were similar to the simple two-component models, except that the models were fitted to two separate subsamples within the sample of data points: the points with $T_{dc} < 20\,K$ and those with $T_{dc} \geq 20\,K$. Having two subsamples allowed a better fit to the $T_{dc} \geq 20\,K$ points; the fits are normally dominated by the $T_{dc} < 20\,K$ subsample of points, often preventing good fits to the $T_{dc} \geq 20\,K$ points. The resultant parameter values for all the model fits are summarized in Table 1. (Notice that the two-component model results for the $T_{dc} \geq 20\,K$ subsample are shown for the two-subsample, two-component models, whereas in Table 2 of Paper I the one-component model results were shown for this subsample.)

To check the results, the systematics were tested. This was done by applying scale factors to the model curves that represented the effect of systematic uncertainties. These were the uncertainties most directly related to the comparison between the model curves and the observational data: the calibration of the observed $I_\nu(240\,\mu m)/I(^{13}CO)$ ratio, the uncertainty in the dipole moment of CO, the uncertainty in the ^{13}CO abundance, and the uncertainty in the dust optical depth to total gas column density. A very rough uncertainty of 20% was adopted for each of these uncertainties (see Paper I for details). These uncertainties are independent and, when added in quadrature, give a total systematic uncertainty of 40%

for the ratio of the model curve to the observed data. Therefore, the scale factors applied to the model curves ranged between 0.6 and 1.4. They were chosen to change in steps of 0.2; the scale factors used were 0.6, 0.8, 1.0, 1.2, and 1.4. Each scale factor was multiplied by the model curve before each fit for all the model types. This gave a range of fitted values for each parameter and this range represents the systematic uncertainty for the given parameter.

For the two-component models an additional test was to slightly shift the starting search grid before running each fit. This also gave a range of results that was comparable to the range found from changing the scale factor.

As a further check on the results, masses and beam filling factors were derived for each of the model types. Specifically, the gas-derived column densities were compared against the dust-derived column densities as a self-consistency check: if the model curve acceptably fit the data in the r_{240} versus T_{dc} plot, then there should be little scatter in the column density versus column density plot. As an additional check, the beam filling factors should be physically meaningful; they should be ≤ 1, given that they are area filling factors.

One flaw of the above-mentioned tests is that they cannot guarantee that the true values are within the ranges of results found from changing the scale factor or the starting grid. The method employed here could be biased to ranges of results that are far from the correct values. Consequently, a third series of tests was performed by fitting the one- and two-component models to simulated data (see Paper II). The results of the modeling and the tests are listed in Table 2 of Paper II. (See Table 2 of the current paper for an updated version of that table.)

The most basic result of this modeling was that the two-component models fit the data better than the one-component models at the 99.9% confidence level, according to the F-test. The dust-gas temperature difference, ΔT, was found to be zero to within 1 or 2 K. The component-0 dust temperature, T_{d0}, was found to be 18 K (uncertainty to be discussed in Section 3). The other parameters, such as the column densities per velocity interval and volume densities for the two components, were much less certain. This is understandable given that the ^{13}CO J $= 1 \rightarrow 0$ line emission is well approximated by the optically thin, LTE limit for much of the gas of the Orion clouds. Consequently, only rough lower limits could be applied to the densities and rough upper limits to the column densities per velocity interval. The lower limit on the column density per velocity interval of component 1 is simply the column density per velocity interval of the clouds on the scale of the *DIRBE* beam. This lower limit for component 0 is near the lower limit of the master search grid.

One important consequence of the two-component models is that there is about 60% more mass than would be inferred from the simpler one-component models. This extra

material is in the form of cold (i.e. $\sim$ 3–10 K) dust and gas.

3.   Considerations of Systematics

In this section we consider the systematics that are less directly connected with the comparison between models and data. Specifically, we examine the effects of changing various assumptions, including the basic assumption itself, on the results; we see how the results change if we neglect to subtract the background/foreground emission from the data, the effects of the emission of the dust associated with the H I gas, the effects for different values of the spectral emissivity index, the effects of a spatially varying ^{13}CO abundance, the effects of varying the column density per velocity interval or density, and how the signal-to-noise filtering has affected the results.

3.1.   The Effects of No Background/Foreground Subtraction

As stated in Section 2.1 of Paper I, there are uncertainties in the subtraction of the large-scale emission (i.e., on the scale of the entire map shown in Figure 2 of Paper I). This large-scale emission was subtracted from the 140 μm, 240 μm, and H I maps. Even though this uncertainty was estimated to be 10%, it is still a good idea to see how this subtraction affects the model results. This was done by repeating the model in the LTE and LVG, one-component cases and in the LVG, two-component case (entire subsample) for the data with*out* the background/foreground subtraction. The results were roughly similar to scaling up the data or, equivalently, scaling down the model curve. As such, the model results in the tested cases were roughly equivalent to those obtained for data that did indeed have the subtraction of the large-scale emission with a scale factor of about 0.9 applied to the model curve. Consequently, *the systematic uncertainty in the observed data is much smaller than that of the total adopted calibration uncertainty of 40%.* This therefore implies that any reasonable estimate of the uncertainty in determining the appropriate level of the large-scale emission to be subtracted will have an even smaller effect on the model results (equivalent to adjusting the scale factor by a few percent).

3.2.   The Effects of Dust Associated with HI

Even though the H I has only small column densities on all lines of sight in the Orion fields (i.e. the average N(H I) is 5×10^{20} cm^{-2} for those positions greater than 5-σ in

$I_\nu(140\,\mu m)$, $I_\nu(240\,\mu m)$, and $I(^{13}CO)$), the dust associated with the H I may still have a non-negligible effect on the model results. To test this, the $140\,\mu m/240\,\mu m$ color tempera- ture of the dust was plotted against the atomic gas to molecular gas column density ratio, $N(H\,I)/2N(H_2)$. Figure 1 shows that the dust color temperature tends to about 21 K as the atomic to molecular gas ratio increases. The correlation between the color temperature and the atomic-to-molecular gas ratio has a confidence level of better than 99.99% according to the Spearman rank-order correlation test. (More specifically, the significance of the null hypothesis of zero correlation is less than 10^{-24}.) The curves represent the hypothetical case of having all the dust in the molecular gas at one fixed temperature and all the dust in the atomic gas at some other fixed temperature. The lower curve assumes that the dust asso- ciated with the molecular gas has a temperature of 16.5 K, while the upper curve assumes a dust temperature of 27 K for the molecular-gas-associated dust. Both curves assume that the atomic-gas-associated dust has a temperature of 22.5 K. Both curves together crudely describe the trends in the data. Consequently, both curves together imply that each line of sight either has molecular gas with cold dust, with $T_d = 16.5$ K, or with warmer dust, with $T_d = 27$ K, along with atomic gas that has dust with a constant temperature of 22.5 K for every line of sight. The variations in dust color temperature would then be largely due to the variation in the atomic-to-molecular gas ratio (along with some scatter). This contradicts the picture represented by the models applied to the r_{240} versus T_{dc} plot. In that picture, the dust in the molecular gas does indeed vary in temperature from one line of sight to another, at least for the dominant component (i.e., component 1).

To resolve this discrepancy, the simulated maps discussed previously were modified by adding a layer of H I and its associated dust with uniform properties throughout: a constant column density of $5\times10^{20}\,H\,atoms\,cm^{-2}$ and a constant dust temperature of 22.5 K. Noise was added to the H I column density map that was the same as the value for the observed H I map. The $140\,\mu m$ and $240\,\mu m$ intensities for this H I layer were computed and added to the original noise-free maps. The noise for the new continuum maps, that include the H I layer's dust emission, was then recomputed from the prescription used previously (i.e., expressions 1 and 2 of Paper II). The results are plotted in Figure 2 in the form of $140\,\mu m/240\,\mu m$ color temperature versus atomic-to-molecular gas ratio, analogous to Figure 1. The simulated data does indeed reproduce the overall shape of the observed data, despite the lack of scat- ter in the former compared to the latter. This scatter in the simulated data can be increased realistically by including variations in the H I column density map and in its dust temper- ature. Nevertheless, it is clear that having *only* two possible constant dust temperatures in the dust associated with the molecular gas is *not* necessary for explaining the trends in Figure 1. Figure 2 shows the same overall trends even though it uses model results that allow a changing dust temperature in the molecular gas.

The question remains as to the size of the change in the model results because of this HI layer and its dust. This question has already been answered indirectly in the previous subsection, the subsection that dealt with the effects of no subtraction of the background/foreground (i.e., large-scale) emission. Such a subtraction was necessary for the continuum maps (i.e., maps of dust emission) and for the HI map (i.e., map of atomic gas emission), but not for the ^{13}CO map. Therefore, the dust emission on the large scale is associated almost completely with the HI gas and *not* with the molecular gas. Accordingly, *not* subtracting the large-scale emission from the continuum maps is equivalent to piling on the atomic gas and its associated dust. In fact, it is equivalent to increasing the quantity of the *HI-associated* dust by factors of 4 to 5 over that in the background/foreground-subtracted maps. And yet, as described previously, the effect of this extra dust (*not* associated with molecular gas) was to change the results of the models (that *only* considered the dust associated with molecular gas) in a way consistent with changing the scale factor by only about 10%. Therefore, the small amount of HI gas and its associated dust that remains in the background/foreground-subtracted maps will have an even smaller effect on the model results — equivalent to changing the scale factor by about 2 to 2.5%. It follows that the changes to the model results will be equivalent to only a tiny fraction of the full range of values for each parameter that is seen in such figures as Figure 21 of Paper I or in Table 2. (Or in the case where there are only lower limits, such as those for the densities listed in Table 2, those lower limits would be essentially unchanged.)

3.2.1. The HI-Associated Dust and the Lower Temperature Limit of the Cold Dust and Gas

One important point that remains is whether the dust associated with the HI is responsible for the model result that there is cold dust and gas at temperatures as low as $3\,\mathrm{K}$. If so, then this result is incorrect. As discussed before, the HI-associated dust has little *overall* effect on the majority of the plotted points. However, this does not mean that the effect of this dust is negligible in *every sub-grouping* of points. Specifically, the vertical section of the model curve in the r_{240} versus T_{dc} plot (see Figures 20 and 24 of Paper I) that represents this very cold material is located between $\mathrm{r}_{240} \simeq 25$ and about $50\,\mathrm{MJy \cdot sr^{-1} \cdot (K \cdot km \cdot s^{-1})^{-1}}$ for $\mathrm{T}_{dc} \simeq 18\,\mathrm{K}$. If the r_{240} values were lower in this part of the plot, then no point would correspond to this "cold" section of the model curve. And the r_{240} values would indeed be lower if the effect of this HI-associated dust were removed, thereby allowing a higher lower limit on the gas and dust temperature of component 1 — i.e., lower limits on T_{K1} and T_{d1} higher than $3\,\mathrm{K}$. Figure 3 shows plots of r_{240} versus the HI fraction (i.e. $\mathrm{N(HI)}/[\mathrm{N(HI)}+2\mathrm{N(H_2)}]$) for the positions with T_{dc} between 17 and 19.5 K and with signal-to-noise ratios greater than

or equal to 5 at $140\,\mu$m, $240\,\mu$m, in the ^{13}CO J $= 1 \rightarrow 0$ line, and greater than or equal to 3 in the H I 21-cm line. These plots show a clear correlation (better than 99% confidence from the Spearman rank-order correlation test), suggesting that the higher r_{240} values are indeed due to dust associated with the atomic hydrogen. The question is how strongly the H I-associated dust is contributing to the total $240\,\mu$m emission. This allows us to correct for the emission of this dust, thereby effectively giving us only the continuum emission and line emission from the molecular gas alone.

Estimating the appropriate correction to r_{240} for the H I associated dust is far from straightforward. One way is to make the crude assumption that the dust-emissivity per H-nucleon of the H I-associated dust, ϵ_{HI}, and for the H$_2$-associated dust, ϵ_{H2}, are each constant for all the positions in the subsample of points to be tested. This subsample is part of the sample used throughout this paper — signal-to-noise greater than or equal to 5 for $I_\nu(140\,\mu$m), $I_\nu(240\,\mu$m), and I(^{13}CO) — with the additional criteria mentioned above:

a) Integrated intensity of the H I line greater than or equal to 3σ.

b) T_{dc} between 17 and 19.5 K.

c) r_{240} between 25 and $50\,\mathrm{MJy \cdot sr^{-1} \cdot (K \cdot km \cdot s^{-1})^{-1}}$.

The $240\,\mu$m specific intensity, $I_\nu(240\,\mu$m), can be represented as

$$I_\nu(240\,\mu\mathrm{m}) = \epsilon_{HI}\,N(HI) \; + \; 2\epsilon_{H2}\,N(H_2) \qquad . \tag{1}$$

Simple linear regression in three dimensions can be used to solve for the emissivities, ϵ_{HI} and ϵ_{H2}, where we fit an equation of the form

$$z = ax \; + \; by \qquad , \tag{2}$$

solving for the optimal values of the coefficients a and b. Since normal linear regression only uses the uncertainties in the z values, the fit should be repeated after interchanging the z values with the x values (and thereby using the x-uncertainties) and then again after interchanging the original z values with the y values (and thereby using the y-uncertainties). This gives us three fits. For the first fit, the $I_\nu(240\,\mu$m) are the z and the uncertainties in $I_\nu(240\,\mu$m) are used in the fitting, $N(HI)$ is x, and $2N(H_2)$ is y. The coefficients a and b then directly correspond to ϵ_{HI} and ϵ_{H2}, respectively. The second fit has $N(HI)$ as z, the uncertainties in $N(HI)$ are used in the fitting, $I_\nu(240\,\mu$m) is x, and $2N(H_2)$ is still y. After solving for the optimum a and b values, expression (2) is rearranged to the form of (1) in order to solve for ϵ_{HI} and ϵ_{H2} in terms of a and b. The third fit is similar to the second fit, but with $2N(H_2)$ as z, $N(HI)$ as x, and $I_\nu(240\,\mu$m) as y. Again, with the resultant a and b values,

the expression (2) is rearranged to the form of (1) and ϵ_{HI} and ϵ_{H2} are found. (Another way to include the errors from all three quantities is to use the orthogonal regression method described at the beginning of Section 3 of Paper I.) In principle, the three different values determined for each of the emissivities can be used as a measure of their uncertainties.

In practice, none of the fits were very good. The fits were applied using the molecular gas column densities (i.e., $N(H_2)$) derived from the one-component, non-LTE models and those using those column densities derived from the two-component, two-subsample, non-LTE models. Typical *reduced* chi-square values were from 30 to 200, although one was as low as $\chi^2_\nu \simeq 6$. None of the fits using the two-component model column densities had reduced chi-square values less than 80. The poor quality of the fits reflects the invalidity of the assumption of spatially constant emissivities. If we nonetheless use the one fit with the *least un*acceptable χ^2_ν value of about 6, then $\epsilon_{H2} \simeq 5\,\epsilon_{HI}$. Given that the maximum atomic gas fraction is about 0.3 (see Figure 3), the H I-associated dust contributes less than about 7% to the total $240\,\mu$m emission. If we tighten criterion c) above to r_{240} between 40 and $50\,\mathrm{MJy \cdot sr^{-1} \cdot (K \cdot km \cdot s^{-1})^{-1}}$ to see how the results are changed, and if we ignore the fits with $\chi^2_\nu \gtrsim 10$ or with a negative value of either ϵ, then we find that $\epsilon_{H2} \simeq 9\,\epsilon_{HI}$. The least unacceptable fits suggest that the H I associated dust makes a contribution of about 3 to 7% to the $240\,\mu$m emission. This result is similar, at least qualitatively, to the result found previously that the H I-associated dust emission has a negligible effect on whole sample of high signal-to-noise points.

Given that no fit was acceptable, at least a simplistic correction should be applied to see what changes to the lower limit of the dust and gas temperature of component 1 are *possible*. The simplest kind of correction is to assume that the emissivities per H-nucleon are equal for the H I-associated dust and the H_2-associated dust, a much more extreme correction than the fits to equation (1) would suggest. Accordingly, the observed $I_\nu(240\,\mu$m) values, and therefore the r_{240} ratio values, must be scaled by $2N(H_2)/[N(H\,I)+2N(H_2)]$. These correction factors were applied, using the one-component values for the molecular gas column densities. This is obviously not consistent with the two-component model results that predict the cold gas and dust. However, assuming correction factors from the one-component model column densities results in more extreme (i.e. further from unity) values of the correction factors that permit a greater appreciation of the tight constraint on the lower temperature limit. These correction factors were applied to the whole sample of high signal-to-noise positions — specifically, all the points with $I_\nu(140\,\mu$m), $I_\nu(240\,\mu$m), and $I(^{13}CO)$ greater than 5σ. Since the H I data were used, criterion a) reduced the sample to 609 points. The uncertainties in the correction factors were *not* propagated to the error bars in the r_{240} values in the sample. The larger error bars in the r_{240} ratios would have produced an ambiguity in the interpretation of the results: was the change in the lower temperature limit of component 1

really due to the correction for the H I-associated dust or was this simply due to the larger error bars? The results of fitting the two-component models to the corrected data should not be taken literally in any case and only point to the potential effects of correcting for the unwanted continuum emission. We are testing the hypothetical case of observing imaginary molecular clouds absolutely free of atomic hydrogen and its associated dust.

The results of fitting a simple two-component model to the H I-corrected data are consistent with the previous two-component model results in Section 3.3 of Paper I. In particular, the results of these corrected models are within the range of values depicted in Figure 21 of Paper I (ignoring the c_o versus scale factor and the $\frac{N_{c0}}{\Delta v_c}$ versus scale factor plots in favor of the $c_o \frac{N_{c0}}{\Delta v_c}$ product versus scale factor plot), except that the density n_{c0} is as small as $10\,\mathrm{cm}^{-3}$. One noteworthy difference is that χ_ν^2 is higher for the two-component model fitted to the corrected data, $\chi_\nu^2 = 6.41$, than for the model fitted to the uncorrected data, $\chi_\nu^2 = 5.69$. If we now increase the lower temperature limit of component 1 from $2.8\,\mathrm{K}$ to $5\,\mathrm{K}$ and search for the optimum parameter values again, then χ_ν^2 increases to 7.54. Specifically, we set the lower limits of T_{K1} to $5\,\mathrm{K}$ and of ΔT to $0\,\mathrm{K}$, resulting in both T_{K1} and $T_{d1} \geq 5\,\mathrm{K}$. Again keeping in mind that the points in the sample are not completely independent, the effective number of degrees of freedom is about 60. Adopting this number, the F-test tells us that raising the lower limit of component-1 temperature to $5\,\mathrm{K}$ can only be rejected at a confidence level of nearly 75%. Such a confidence level does not inspire much confidence, and we should probably accept the fit. Consequently, it is *possible* that gas and dust with temperatures between 3 and $5\,\mathrm{K}$ are not necessary for explaining the observations. If this is the case, then the correction factor of 1.6 to the one-component masses would have to be corrected downward.

In general, it *seems* that the H I-associated dust can*not* provide an alternative explanation for the cold dust and gas (i.e. temperature between 3 and $10\,\mathrm{K}$). Nonetheless, there is a possibility that the lower limit of the component-1 temperature is about $5\,\mathrm{K}$ instead of $3\,\mathrm{K}$. Then the estimated fraction of the total gas mass in the cold portion would be less than the original estimate of about 40-50%.

3.3. Varying X(^{13}CO)

Warin et al. (1996) examined the photodissocation and rotational excitation of CO and its isotopologues in diffuse, translucent, and dense dark clouds. They found that the ^{13}CO/^{12}CO abundance ratio (i.e. X(^{13}CO)/X(^{12}CO)) can vary by factors of 2 or 3 as a function of depth into the cloud (see the left-most panel of their Figure 16). Given that T_d varies with N(H I + 2H$_2$) in the Orion clouds (e.g., see Fig 4 of Paper II), is it then possible that the

observed variation of r_{240} with T_d is because $X(^{13}CO)$ is varying with $N(H I + 2H_2)$? Examining the $I(^{13}CO)/I(^{12}CO)$ as a function of $N(H I + 2H_2)$ (an approximation of their Figure 16) shows no consistent trend and is at odds with the results of Warin et al. (1996). Therefore, it is very *un*likely that variations of $X(^{13}CO)/X(^{12}CO)$ could account for the *overall* trends seen in r_{240} versus T_d.

Nevertheless, variations in $X(^{13}CO)/X(^{12}CO)$ could still explain unusually small or large r_{240} values for some points in the r_{240} versus T_d plots. In particular, the points near the top of the triangular cluster could be explained by a lower $X(^{13}CO)$. This is discussed in detail in Section 4.5.

3.4. Models with $\beta \neq 2.0$

Johnstone & Bally (1999) find that the dust emissivity index, β, might have a range as extreme as from 1.5 to 2.5 in Orion A. Two-component models using adopted values of 1.5 and 2.5 for β were applied to the data to see the effects on the results. The resultant parameter values were consistent with the ranges of values listed in Table 2, with one exception: the range of T_{d0} values is changed because β is different from before — all the inferred dust temperatures are changed. For $\beta = 1.5$, $T_{d0} = 21\,K$ was found and, for $\beta = 2.5$, $T_{d0} = 16\,K$ was the best fit.

In short, with the exception noted above, the resultant parameter values are still within the range of values expected from the scale factor variations. Thus the most extreme variations of β still largely give model results within the ranges listed in Table 2.

3.5. Models with Varying $N(^{13}CO)/\Delta v$ or Varying $n(H_2)$

These were essentially one-component models with only three parameters on any *one given line of sight:* ΔT, $N(^{13}CO)/\Delta v$ and $n(H_2)$. The approach here was to vary not only the T_d and T_K from one line of sight to another (keeping ΔT constant), but also to vary one of two parameters: the column density per velocity interval ($N(^{13}CO)/\Delta v$) or the density ($n(H_2)$). To characterize all the lines of sight represented in the r_{240} versus T_d plot, there were 9 parameters in total for a curve that was strongly decreasing through the triangular cluster of points at low T_d, gently rising for the intermediate T_d, and then strongly rising for high T_d. Thus there were 3 intervals of T_d that were delimited with 4 parameters: T_1, T_2, T_3, and T_4. If we consider first only the models with varying $N(^{13}CO)/\Delta v$, then on the first interval, $[T_1, T_2]$, the $N(^{13}CO)/\Delta v$ was equal to N_1 at T_1 and to N_2 at T_2 and the $N(^{13}CO)/\Delta v$ value

at any point in this interval was determined by logarithmically interpolating between N_1 and N_2. The same approach was used on the last interval, $[T_3, T_4]$, with $N(^{13}CO)/\Delta v$ values equal to N_2 at T_3 and to N_3 at T_4. On the interval $[T_2, T_3]$, $N(^{13}CO)/\Delta v$ was held constant at a value of N_2. The fitted parameters were then ΔT, T_1, T_2, T_3, T_4, N_1, N_2, N_3, and the fixed density, n (with best-fit values of $0 \pm 1\,\mathrm{K}$, $16 \pm 1\,\mathrm{K}$, $17 \pm 1\,\mathrm{K}$, $24 \pm 1\,\mathrm{K}$, $27 \pm 1\,\mathrm{K}$, $(5 \pm \frac{3}{2}) \times 10^{16}\,^{13}CO\,molecules \cdot \mathrm{cm}^{-2} \cdot (\mathrm{km \cdot s}^{-1})^{-1}$, $(2 \pm \frac{1}{?}) \times 10^{14}\,^{13}CO\,molecules \cdot \mathrm{cm}^{-2} \cdot (\mathrm{km \cdot s}^{-1})^{-1}$, $(8 \pm 5) \times 10^{16}\,^{13}CO\,molecules \cdot \mathrm{cm}^{-2} \cdot (\mathrm{km \cdot s}^{-1})^{-1}$, and $(3 \pm \frac{2}{1}) \times 10^3\,H_2\,molecules \cdot \mathrm{cm}^{-3}$, respectively). Achieving a reasonable-looking "best" fit presented a number of problems:

1. The fitting is heavily biased towards the low-T_d points (i.e., $T_d \lesssim 21\,\mathrm{K}$). The points with $T_d \gtrsim 22\,\mathrm{K}$ are almost excluded in the model fits.

2. Even within the low-T_d points, the fits tend to bypass the central area of the large triangular cluster of points.

3. There is a very large hump in the model curve for T_d around $22\,\mathrm{K}$ that overestimates the data points by more than an order of magnitude.

4. The best fit for N_2 is more than order of magnitude lower than the observed large-scale $N(^{13}CO)/\Delta v$ value (see Section 3.2 of Paper I).

5. In order to fix the bias towards the low-T_d points and remove the hump, it was necessary to apply weights to the data to reduce or remove this bias. This resulted in a chi-square value that was somewhat subjective, given that the choice of weights was somewhat subjective.

The models with varying $n(H_2)$ had similar, though not identical, problems. For these models, the $N(^{13}CO)/\Delta v$ parameters interchange with the $n(H_2)$ parameters: ΔT, T_1, T_2, T_3, T_4, n_1, n_2, n_3, and the fixed column density per velocity interval, N (with best-fit values of $-2 \pm 1\,\mathrm{K}$, $14 \pm 1\,\mathrm{K}$, $18 \pm 1\,\mathrm{K}$, $22 \pm 1\,\mathrm{K}$, $30 \pm 1\,\mathrm{K}$, $10 \pm \frac{8}{?}\,H_2\,molecules \cdot \mathrm{cm}^{-3}$, $(5.6 \pm \frac{4.4}{2.5}) \times 10^4\,H_2\,molecules \cdot \mathrm{cm}^{-3}$, $10 \pm \frac{8}{?}\,H_2\,molecules \cdot \mathrm{cm}^{-3}$, and $(2 \pm \frac{1}{?}) \times 10^{15}\,^{13}CO\,molecules \cdot \mathrm{cm}^{-2} \cdot (\mathrm{km \cdot s}^{-1})^{-1}$, respectively). As with the models mentioned in the previous paragraph, these models have biases that inhibit good fits through the $T_d \gtrsim 22\,\mathrm{K}$ points or through the central part of the triangular cluster. However, the problems for $n(H_2)$-varying models differ in three ways from those of the $N(^{13}CO)/\Delta v$-varying models:

- The hump for the $N(^{13}CO)/\Delta v$-varying models centered at about $T_d = 22\,\mathrm{K}$ is much smaller for the $n(H_2)$-varying models. This hump for the latter models only overestimates the data by about a factor of 2.

- The best-fit $N(^{13}CO)/\Delta v$ value is still low, but is now within a factor of 2 of the lower limit imposed by the large-scale observed $N(^{13}CO)/\Delta v$ value.

- The best way to reduce the bias towards the low-T_d points was to fix the T_1, T_2, T_3, and T_4 values. The choice of these values and their uncertainties was somewhat subjective.

The best-fitting model curve gave a reduced chi-square of 9.2.

While the best of these models is much better than the one-component models that used the basic assumption (i.e., $\chi^2_\nu = 16.5$ and 16.9), it is still much worse than the two-component models (i.e., $\chi^2_\nu = 5.7$ and 5.3). In addition, the models with varying $n(H_2)$ (or varying $N(^{13}CO)/\Delta v$) require subjective judgement in determining the values to fix for some of the parameters (or in adjusting the weights of different subsamples of data points). And despite having fewer parameters (9 as opposed to 15) than the two-component, two-subsample models — the most elaborate of the models that obey the basic assumption (within each subsample at least) — the models with varying $n(H_2)$ or varying $N(^{13}CO)/\Delta v$ are actually *more* complicated than these two-component models. They are more complicated because these models essentially divide up the sample of data points into *three* subsamples instead of two, and two of these subsamples (in intervals $[T_1, T_2]$ and $[T_3, T_4]$) allow $n(H_2)$ (or $N(^{13}CO)/\Delta v$) to vary in addition to T_d (along with T_K so as to keep ΔT constant). In contrast, the two-component, two-subsample models have only T_d varying (along with T_K so as to keep ΔT constant) within each subsample — the basic assumption is obeyed in each subsample.

In short, relaxing the basic assumption by using models with simple systematic variations of either $N(^{13}CO)/\Delta v$ or of $n(H_2)$ results in poorer, and more subjective, fits than the best models following this assumption.

3.6. Signal-to-Noise Considerations

Given that the sample of points modeled in the r_{240} versus T_{dc} plots represents only 25.8% of the Orion Fields, how well does this sample represent the physical conditions in the Orion clouds as a whole? A related question is what fraction of the positions that have gas/dust emission from the Orion clouds is represented by the sample? The contour maps in Figure 2 of Paper I suggest that roughly three-quarters of the Orion Fields have gas and dust. Some low-level emission could come from elsewhere along the line of sight, so maybe only half of the Orion Fields are occupied by the Orion clouds. However, even in this extreme possibility, the modeled positions still only represent about 50% of the Orion clouds' area — still *not* a majority of the positions. Clearly, just how strongly the inferred physical conditions depend on the signal-to-noise threshold used in sample selection must be tested.

The most straightforward test, namely lowering the signal-to-noise threshold until most of the Orion Fields are represented, is not practical. There would be 2 to 4 times the number of points to fit and the majority of these would have huge error bars. Consequently, this sample of points would be difficult to model reliably. The alternative test is to raise the signal-to-noise threshold and see how the inferred physical conditions change with this threshold. This has the disadvantage of going from a minority of the points to an even smaller minority. Nonetheless, this alternative has the very strong advantage that only very high signal-to-noise points are modeled, thereby yielding more reliable fit parameters.

To do this alternative test, the threshold was increased appreciably: from 5σ to 20σ in $I_\nu(140\,\mu m)$, $I_\nu(240\,\mu m)$, $I(^{13}CO)$. This sample has only 6.6% of the Orion Field positions. An LVG, two-component model was fitted to this sample. The resultant parameter values were consistent with those specified in Table 2, with one notable exception: T_{d0} was $17\,K$ instead of the usual $18\,K$. This change in the component-0 dust temperature is not surprising. The signal-to-noise ratio is proportional to the surface brightness, and this depends mostly on the gas/dust column density. So signal-to-noise ratio is roughly equivalent to depth into the clouds. Increasing this ratio's threshold is almost like filtering out the cloud edges and looking more deeply into the clouds. The T_{d0} is the roughly constant temperature on the scale of the Orion clouds of some dust component. If this dust component is on the surfaces of the clouds, then it is the temperature of the dust heated primarily by the general ISRF. If this dust component is just below the clouds' surfaces, then this is the temperature of the dust heated primarily by an ISRF shielded by the surface layers of gas and dust, resulting in a lower temperature. Then by extrapolation, modeling of *all* the positions in the Orion Fields (if there were sufficient signal-to-noise) could yield $T_{d0} \simeq 19\,K$.

Accordingly, modeling the full spread of points in the r_{240} versus T_{dc} plot probably requires a spread in the physical parameter values that have been held constant. For example, the horizontal spread of the triangular cluster in an r_{240} versus T_{dc} plot (e.g., see Figure 20 of Paper I) probably means a component-0 dust temperature varying between about 16 and $19\,K$. (As such, an updated version of Table 2 of Paper II becomes Table 2 of the current paper, which includes this estimate of the range of T_{d0} values.) Analogously, other parameter values, such as the densities and column densities per velocity interval, must also vary to "fill" the space occupied by the sample of points, as suggested in Section 3.5 of Paper I. Nonetheless, the current modeling effort is a sufficient first approximation.

The most important result of varying the signal-to-noise ratio is that the sample with only 25.8% of the Orion Field positions *may* indeed represent the bulk of the Orion clouds. There was no appreciable change (except a slight change in T_{d0}) in going from the factor of $\sim$4 from 6.6% of the fields to 25.8%. Therefore, extrapolating the extra factor of $\sim$4 to

100% *may* also yield no appreciable change. This is far from certain, of course, because the extrapolation from 25.8% to 100% could cross some depth threshold that appreciably alters the parameter values. On the other hand, the effective spatial resolution of these observations is 8 pc at the distance of the Orion clouds. Averaging over such large size scales may reduce the effects of varying the sample.

In short, varying the signal-to-ratio used in selecting the sample may have little effect on the derived gas/dust physical conditions.

4. Scientific Implications and Discussion

The astronomical implications of the results are numerous and include modifications to models of dust/gas thermal coupling, to estimates of mass and kinetic temperature of molecular gas on galactic scales, and to our understanding of the X-factor to name a few. These issues and others will be discussed in the following sections (or in subsequent papers as for the X-factor), after discussing the appropriateness of using the LVG models.

4.1. Use of the LVG Code

Some literature suggests that the LVG models can give inconsistent results and that photodissociation region (PDR) models remove the inconsistencies (e.g., Mao et al. 2000). The PDR models represent a nearly complete explanation for the emission strength of molecular lines, whereas the LVG models merely relate the molecular line strength to simple physical parameters in a simplified case. Consequently, the PDR models should yield more reliable estimates of physical parameters like temperature and density than those of the LVG models. However, some papers that use CO line ratios to claim that the LVG model results are unsatisfactory compared with those of PDR models often suffer from flawed and inconsistent arguments.

Mao et al. (2000), for example, model the physical conditions in the central ~ 500 pc of the galaxy M 82. They claim that their CO data yield physically unreasonable results when using the LVG models — results that supposedly become more reasonable when using PDR models. The problems with this claim is summarized below. They state, among other things, that the LVG models imply gas densities that are too low, cloud sizes that are too large, and area filling factors that are inconsistent with volume filling factors. Their first claim of low gas densities is connected with their restriction of the $X(^{13}CO)/(dv/dr)$ value. They use the observed *large-scale* velocity width of the lines compared with the size of

the observed region to fix the numerical value of $X(^{13}CO)/(dv/dr)$ within a narrow range. However, the large-scale (i.e., on the scale of the beam) $X(^{13}CO)/(dv/dr)$ has little to do with this parameter value within the individual clumps responsible for much of the observed emission. If their approach *were* also applied to the volume density, then it *would have been* equivalent to dividing the mass of gas within the beam by the volume of this gas to estimate and fix the gas density, which is well known to be only a rough lower limit to the density within the clumps. They did not make this mistake, but did make the equivalent mistake for the $X(^{13}CO)/(dv/dr)$ value. Had they allowed $X(^{13}CO)/(dv/dr)$ to vary over a wider range, they would have satisfied the density constraints suggested by the other observations they mentioned. Their second claim of overly large cloud sizes implied by the LVG model results was based on two different methods. Both methods, however, overestimated the cloud sizes by the ratio of the observed line velocity width to the cloud velocity width, which is about an order of magnitude. One method was dividing the column density of a single cloud by its volume density, where both the column density and volume density were LVG results. The second method estimated volume and area filling factors from LVG results, their ratio giving the size of a single cloud. Both methods were applied incorrectly. The first method converted from $N(^{13}CO)/\Delta v$ to cloud $N(H_2)$ by using the *entire* observed line width, which also includes the rotation of the observed galaxy, instead of using an estimate of a cloud line width (i.e. 5-10 km $\cdot$ s^{-1}). The second method suffered from the same overestimate. The cloud size depends on the ratio of the volume to area filling factors, but the area filling factor *must be* for *all* the gas at *all* the velocities within the line profile (assuming that there is never more than one cloud on any line of sight for *all* the velocities within the line profile). However, they clearly used the ratio of the observed line strengths to those of the model, which gives the area filling factor *within a narrow velocity interval* and *not* the area filling factor over the entire line profile. This second method must include the ratio of the cloud velocity width to the line velocity width, again reducing the estimated cloud size by an order of magnitude. The third claim of inconsistent area and volume filling factors is weak at best, given that the relationship between the two is not a fixed, straightforward expression that applies in every case. If we nonetheless accept the expression used by Mao et al. (2000), then there was indeed a minor discrepancy between the two types of filling factor for the LVG model results. However, what Mao et al. (2000) ignored entirely was that *the corresponding discrepancy for the PDR models is* **much** *larger than that for the LVG model results.* The filling factor argument was applied in a clearly biased manner. In short, all three claims are based on arguments that are faulty or biased or both.

In addition to the problems above, there is the strong evidence provided by Weiss et al. (2001): they used data similar to those of Mao et al. (2000) and recovered the same physical conditions, *while using only LVG models.* Obviously, if Weiss et al. (2001) and Mao et al.

(2000) agree on the physical conditions, then they disagree on the necessity of the PDR models for recovering those conditions. And given that Weiss et al. (2001) recovered those conditions with only the LVG models, then the claim of Mao et al. (2000) that PDR models are necessary is clearly incorrect. Therefore, the LVG models are *clearly as reliable* as the PDR models when using CO lines (at least on scales of a few or more parsecs).

Consequently, the LVG models applied to the large-scale physical conditions in the Orion molecular clouds, as described in this paper, are also as reliable as the PDR models.

4.2. Comparison of Derived T_K, $n(H_2)$, and $N(^{13}CO)/\Delta v$ with Previous Work

There are few papers that discuss the molecular gas physical conditions of the *entire* Orion A and B clouds, as inferred from two or more transitions of CO. Sakamoto et al. (1994) inferred these physical conditions using the $J = 2 \rightarrow 1$ and $J = 1 \rightarrow 0$ lines of ^{12}CO. Of all the rotational lines of ^{12}CO and its isotopologues, these are the *least* sensitive to the gas physical conditions. Nevertheless, they at least provide a rough comparison with the physical conditions obtained in the current paper that used the dust-continuum to gas-line ratio. As discussed in Paper II, the ^{13}CO $J = 1 \rightarrow 0$ emission is dominated by that of component 1 in all but the few points with $T_d = T_K \lesssim 4\,K$ in that component. Since this is molecular gas emission, this emission, rather than the FIR continuum, better identifies the component with which to compare single-component model results, such as those of Sakamoto et al. (1994). Consequently, the component-1 parameters in Table 2 are compared with the Sakamoto et al. (1994) results.

The physical conditions inferred by Sakamoto et al. (1994) are consistent with those inferred in the current paper. They found the following physical conditions in the Orion molecular clouds:

— $N(^{12}CO)/\Delta v$ between about 1×10^{16} and about 3×10^{18} ^{12}CO $molecules \cdot cm^{-2}$, which corresponds to $N(^{13}CO)/\Delta v$ between about 2×10^{14} and 5×10^{16} ^{13}CO $molecules \cdot cm^{-2}$,

— $n(H_2) \gtrsim 3 \times 10^3\,cm^{-3}$ over much of the clouds' areas, except for $n(H_2) \simeq 2 \times 10^2\,cm^{-3}$ in the clouds' peripheries,

— T_K between $10\,K$ and $40\,K$, the latter temperature found near the H II regions.

Sakamoto et al. (1994) chose to do their LVG analysis with diagrams of constant $X(^{12}CO)/(dv/dr)$ instead of constant $N(^{12}CO)/\Delta v$. They considered only values of 1×10^{-4}

and $1 \times 10^{-5} \, (\mathrm{km \cdot s^{-1} \cdot pc^{-1}})^{-1}$. Given that the ^{13}CO J $= 1 \to 0$ clumps have velocity widths and sizes consistent with dv/dr of a $few \, \mathrm{km \cdot s^{-1} \cdot pc^{-1}}$ (see Nagahama et al. 1998), the maximum X(^{12}CO)/(dv/dr) value should be a $few \times 10^{-5} \, (\mathrm{km \cdot s^{-1} \cdot pc^{-1}})^{-1}$, given the ^{12}CO abundance mentioned in Appendix A of Paper I. Also, given that some structures have dv/dr of around $100 \, \mathrm{km \cdot s^{-1} \cdot pc^{-1}}$ — even though seen with other tracers like CH$_3$OH (Cernicharo et al. 1999) these structures are nonetheless real — the minimum X(^{12}CO)/(dv/dr) should be around $10^{-6} \, (\mathrm{km \cdot s^{-1} \cdot pc^{-1}})^{-1}$. Nevertheless, because such structures have higher densities than those normally inferred from CO observations on parsec scales, the range of N(^{13}CO)/Δv values are probably still roughly those of Sakamoto et al. (1994). This range is larger than the range of $\frac{\mathrm{N_{c1}}(^{13}\mathrm{CO})}{\Delta\mathrm{v_c}}$ values listed in Table 2, but includes the range listed in that table. The upper limits of N(^{13}CO)/Δv for Sakamoto et al. (1994) and for Table 2 are similar to within a factor of 3, but the lower limits differ by more than an order of magnitude. This disagreement is probably because Sakamoto et al. (1994) did not use the large-scale N(^{12}CO)/Δv of the entire cloud as a rough lower limit on that of the clumps. Their densities are consistent with the lower limit in Table 2 for component 1, except for their density for the peripheries. This density is consistent with the lower limit we found for component 0. Accordingly, these peripheral regions may represent a low-density envelope surrounding the entire clouds and are seen in projection along the clouds' edges. The clumps in this envelope may be, in fact, the component 0 of the current paper.

The comparison between the kinetic temperatures of Sakamoto et al. (1994) and those of the current paper is complicated by the high optical depths of the ^{12}CO lines observed by the former. The high optical depths imply that the inferred densities and column densities per velocity interval are biased towards of the surfaces of clumps. This is especially true for the inferred kinetic temperatures, because, in the optically thick case, these temperatures are more directly related to the observed line radiation temperatures than are the other physical parameters. The high optical depths then mean that the warmer component will dominate the ^{12}CO emission in these lines. We then simplistically assume that the T$_{dc} < 20$ K subsample is essentially component 0 and that the T$_{dc} \geq 20$ K subsample is component 1. (Note that this is not consistent with the choice of component used to compare the N(^{13}CO)/Δv and n(H$_2$) results. If these other physical parameters had been compared with the component-0 results instead of those of component 1, then the agreement would still have been reasonable, given the loose restriction on the parameters.) With this approximation, the gas kinetic temperatures as sampled by the ^{12}CO are approximately the same as the $140 \, \mu$m/$240 \, \mu$m dust color temperature, T$_{dc}$. Sakamoto et al. (1994) found T$_{\mathrm{K}} = 40$ K near the H II regions and 10–20 K away from the H II regions. The current paper finds T$_d =$ T$_{\mathrm{K}} \simeq 25$ K near the H II regions and 15–20 K away from those regions, a range of values less extreme than, and inside of, that of Sakamoto et al. (1994). The range is less extreme in the latter case because the

spatial resolution is worse by factors of 6 to 7 than those of Sakamoto et al. (1994).

In short, the physical conditions derived here basically agree with the previous results of Sakamoto et al. (1994).

4.3. Column Density Determinations and the Two-Component Models

As found in Paper I (and Paper Ia), the column densities derived from the ^{13}CO J = $1 \rightarrow 0$ line agreed significantly (at a confidence level better than 99.9%) better with those derived from the far-IR continuum for the two-component models than for the one-component models. An important difference between the two components is that component 0 has unvarying gas and dust temperatures from sightline to sightline, whereas component 1 has these temperatures varying spatially (while maintaining a constant dust-gas temperature difference). Thus each sightline has two gas temperatures (and two dust temperatures), except for those few sightlines where the component-0 and component-1 temperatures were the same. Hence, two temperatures along each sightline was necessary for recovering reliable column densities.

This result is similar to that found by Schnee et al. (2006). They compared the continuum-derived column densities with those derived from extinction for the Perseus and Ophiuchus molecular clouds. The scatter in those plots more or less matched that in a simulated cloud that assumed isothermal dust on each sightline. They concluded, therefore, that deriving reliable column densities requires assuming variations of temperature along each sightline. This supports the result of the current work that at least two temperatures are needed on each sightline for estimating reliable column densities.

4.4. $\Delta \mathrm{T} = 0$

The result that the gas and dust temperatures are the same is unexpected, both theoretically and observationally. For example, the theoretical model of PDRs applied to the Orion Nebula and its associated molecular gas (Tielens & Hollenbach 1985,a) predicts $\Delta \mathrm{T} \simeq -70$ to $+20\,\mathrm{K}$ for cloud depths for which the dominant form of carbon is CO (i.e. $\mathrm{A_v} \gtrsim 3\,\mathrm{mag}$). This model, however, does not apply to multi-parsec scales in the Orion clouds: it uses a far-UV radiation field strength of $G_o = 10^5$ and a density of $2.3 \times 10^5\ H\ nuclei \cdot \mathrm{cm}^{-3}$; both are too high for the molecular clouds on larger scales. The far-UV radiation field on such scales is roughly $G_o \sim few$ (see Figure 17 and Section 4.1 of W96) and the density could be as low as $few \times 10^3\ H_2\,\mathrm{cm}^{-3}$ (see Table 1). Consequently, the "standard" PDR model

adopted by Mochizuki & Nakagawa (2000) — which assumes $n(H_2) \sim 10^3 \, \text{cm}^{-3}$, at cloud depths for which H_2 is the dominant form of hydrogen (i.e. $N(H_2) \gtrsim 10^{21} \, \text{cm}^{-2}$), and $G_o = 10$ — is more appropriate for comparison with the work done here and yields $\Delta T \simeq -13$ to $+5 \, \text{K}$. Considering the uncertainty in the ΔT of the current work, these theoretical values are factors of about 5 to 10 too large. Given that there are many heating and cooling mechanisms in PDRs (see Tielens & Hollenbach 1985, for a comprehensive description) with different dependences on the density and on the radiation field (as well as on other quantities), adjusting the theoretical expressions for these many mechanisms to give ΔT near zero would only yield the desired result for an improbably narrow range of physical conditions (i.e., narrow range of G_o and $n(H_2)$ values). On the other hand, simply increasing the gas-dust thermal coupling by the required factor will easily achieve the desired result. This corresponds to the Λ_{gd} function developed by Burke & Hollenbach (1983) and represents a cooling mechanism of the gas due to its collisions with the dust (and, of course if $\Lambda_{\text{gd}} < 0$, it represents a heating mechanism of the gas due to those collisions). Therefore, increasing Λ_{gd} by factors of 5 to 10 can explain the current observations.

A commonly used form of Λ_{gd} is that of Goldsmith (2001) and is given as equation (A10) in Appendix A. Goldsmith (2001) used the Burke & Hollenbach (1983) expression and adopted certain parameter values, including a grain size that was a little too large. Also the Burke & Hollenbach (1983) expression only assumes a single grain size, and not the range of grain sizes that exists in the ISM (see for example Mathis et al. 1977; Désert et al. 1990). When a reasonably realistic range of grain sizes is considered, the Λ_{gd} of Goldsmith (2001) is increased by factors of 3 to 4 (see Appendix A). This is not quite the factor of 5 to 10 desired, but additional increases are easily possible when one considers grains with non-spherical shapes or with projections on their surfaces. As mentioned in Appendix A, Λ_{gd} is proportional to the ratio of the grain geometric cross-section to the grain volume (assuming uniform grain density). If the grains are elongated, then it would be easy to increase this ratio. (In reality it is the cross-section averaged over all viewing angles that is important here. However, even modest elongations of a factor of a few would still result in a larger average cross-section than a sphere with the same volume.) Alternatively, projections on the grain surface could also increase this ratio, but, since the relevant area is the cross-section rather than the total surface area, these projections would have to be large compared to the grain size. In any event, achieving an additional factor of 2 is possible. This would mean that simple geometric considerations could increase the commonly used form of Λ_{gd} by factors of 6 to 8. Therefore, Λ_{gd} can indeed be larger than had been previously assumed and could possibly explain the $\Delta T \simeq 0$ result for the Orion clouds.

Observationally, $\Delta T \simeq 0$ is unexpected as well (e.g., Wu & Evans 1989; Mangum et al. 1999; Lis et al. 2001). As discussed in the introduction, the different temperature and density

sensitivities of the dust continuum emission and gas line emission can result in incorrect inferences of the relative dust and gas temperatures at each point along the line of sight; the continuum and line emission preferentially trace different regions of the ISM within the same line of sight. In addition, in many cases the uncertainty in the dust temperature or in the gas temperature, or both, is large enough that $T_d = T_K$ cannot be ruled out. In Wu & Evans (1989), for example, the uncertainties in T_d were usually $\pm 1\,K$ or $\pm 2\,K$. The uncertainties in T_K were not explicitly listed for some sources, but would be at least about 10% due to the stated calibration uncertainty. Even though they did observe two lines of CO — $J = 1 \rightarrow 0$ and $J = 2 \rightarrow 1$ of ^{12}CO — they did not use their ratio to estimate T_K; as shown in Figure 1 in the introduction of Paper I, this gives only a very *un*interesting lower limit on T_K. Instead, they used the peak radiation temperature of each line, Rayleigh-Jeans corrected and corrected for the cosmic background, to estimate T_K. They assumed the lines to be optically thick and thermalized. However, they also implicitly assumed that the gas fills the beam at the peaks of the lines. As we have found in the current paper, this is not necessarily true, and may not be true even with the superior angular resolution of the Wu & Evans (1989) observations (a factor of 30 to 60 smaller beam). In addition, they used the $60\,\mu m$ and $100\,\mu m$ observations of IRAS. As stated before, the $60\,\mu m$ emission suffers the contamination of emission from stochastically heated dust grains (e.g., Désert et al. 1990, W96). However, because the Wu & Evans (1989) observations are on angular scales of $1'$ to $2'$, the radiation fields on such small size scales could be large enough that the $60\,\mu m$ emission largely comes from grains in thermal equilibrium (i.e., the grains that would be stochastically heated in a normal interstellar radiation field reach thermal equilibrium in a strong radiation field). A crude extrapolation of the trend in the data in Figure 10a of W96 suggests that the column densities derived from 60 and $100\,\mu m$ data will agree with those derived from longer wavelengths for $T_d \simeq 60\,K$. Since $T_d = 18\,K$ for the general ISRF (see W96, Désert et al. 1990), and given that the ISRF is proportional to $T_d^{\beta+4}$, then radiation fields of at least $G_o \sim few \times 10^2$ ensure that the $60\,\mu m$ emission originates largely from grains in thermal equilibrium. One of the sources observed by Wu & Evans (1989), B35, has a radiation field of $G_o \simeq 30$ (Wolfire et al. 1989, and references therein), roughly an order of magnitude too low to exclude the likelihood of stochastically heated grains contributing to the $60\,\mu m$ emission. Therefore, for the source B35, and probably a few others in their list, the derived dust temperature overestimates the dust temperature of the large thermal equilibrium grains. In short, their estimates of T_K are lower limits and their T_d values are likely to be overestimates (especially in the case of B35). Accordingly, their conclusion that the observations are consistent with $T_d > Tk$ for the majority of their sources *still does not exclude the possibility of* $T_d = T_K$ for these same sources.

The same can be said for the observations of Mangum et al. (1999). They observed lines

of formaldehyde, H_2CO, towards dense gas condensations in NGC 2024 in the Orion B cloud with angular resolutions of $12''$, $19''$, and $30''$. They found T_K values from around 50 K to around 250 K. They then compared the derived gas T_K values with the dust temperatures of Mezger et al. (1992), derived from the ratio of the $870\,\mu m$- to the $1300\,\mu m$-continuum emission at resolutions comparable to those of the H_2CO line observations (i.e., $24''$ and $8''$, respectively). These continuum observations imply $T_d = 19$ K. While, at face value, a difference between a T_K of 250 K and a T_d of 19 K may seem substantial, the uncertainties in T_K (see Table 4 of Mangum et al. 1999) suggest that $T_K - T_d$ is significant at levels of only 2 to $4\,\sigma$. These *would be* satisfactory levels of significance, except that the correct uncertainty in $T_K - T_d$ must also include the uncertainty in T_d as well — an uncertainty that was ignored entirely. Mezger et al. (1992) state a 20% uncertainty in their continuum fluxes, implying an uncertainty of about 30% in the $870\,\mu m$ to $1300\,\mu m$ continuum. This uncertainty implies that $T_d = 19$ K is consistent with $T_d = 7$ K to ∞. (Note that, even if we optimistically assume the continuum intensity ratio uncertainty to be only 20%, the upper limit on T_d would still be ∞.) In other words, the continuum observations do *not* place *any* upper limit on T_d. In fact, the difference between 19 K and 250 K corresponds to only a 16% change in the $870\,\mu m/1300\,\mu m$ intensity ratio — a change of ~ 0.5-σ. Therefore, again, the observations *do not exclude the possibility of* $T_d = T_K$.

In contrast, observations of giant molecular cloud cores in the Galactic Center by Lis et al. (2001) seem to genuinely rule out equal dust and gas temperatures. They use continuum observations at a number of wavelengths from 45 to $850\,\mu m$ and observations of the molecular lines of H_2CO, CS and other molecules to determine reliable dust and gas temperatures. They find two components of dust: a warm component with $T_d \simeq 35$ K, which dominates for $\lambda \lesssim 100\,\mu m$, and a cooler component with $T_d \simeq 18$ K, which dominates for $\lambda \gtrsim 100\,\mu m$. (Note that they also estimated the radiation field strength to be $G_o \simeq 500$ to 1000. Therefore, the shorter wavelengths can also give reliable dust temperatures in this case.) The molecular gas temperatures are $T_K \simeq 60$ to 90 K, implying gas-dust temperature difference as high as about 70 K. However, given the appreciable foreground emission towards the Galactic Center and the lack of velocity information from the continuum observations, contamination of these continuum observations by such foreground emission cannot be ruled out. This foreground emission would be from the dust in the Galactic disk and has a temperature of about 18 K (Sodroski et al. 1994). Consequently, only the 35 K dust might be directly associated with the observed cores in the Galactic Center. The molecules observed have transitions with high critical densities $(n_{crit} \gtrsim 10^4\ H_2 \cdot cm^{-3})$ and it could be argued that the observed transitions are only sampling the densest portion of the molecular gas. However, given that the bulk of the gas in the Galactic Center is high-density gas (Bally et al. 1987), the observed transitions are probably sampling most of the molecular

gas in the observed cloud core. Therefore, the gas-dust temperature difference cannot be any smaller than about 25 K, but is probably smaller than 70 K.

Considering the observations, we can draw an important conclusion about ΔT: it seems that $\Delta T \simeq 0$ is *not* excluded for a weak ISRF of $G_o \lesssim 10^2$ and that it *is* excluded for a strong ISRF. Another possibility is that, given that the Galactic Center represents a unique Galactic environment, finding $\Delta T \neq 0$ may have more to do with other physical conditions than simply the strength of the radiation field and the gas density. Nevertheless, for now, a good working assumption is that ΔT is indeed near 0 for $G_o \lesssim 10^2$ and that ΔT is quite different from that, i.e. $|\Delta T| \gtrsim 25$ K, for $G_o \gtrsim 10^3$. If this assumption is correct, then $\Delta T \simeq 0$ on multi-parsec scales for most molecular gas in the Galaxy, and $\Delta T \neq 0$ on these scales in the Galactic Center or in regions with large-scale star formation. This has a number of consequences, including the following:

1. Galactic-scale molecular gas temperatures are nearly double the temperatures previously believed. Applying corrections for the cosmic background and for the Rayleigh-Jeans approximation, the peak radiation temperatures found for the ^{12}CO $J = 1 \rightarrow 0$ line in large-scale surveys of the Galaxy (e.g., Sanders et al. 1985) suggest that $T_{\text{K}} \sim 10$ K. If ΔT is indeed close to zero, then the true T_{K} is close to that of T_d on large scales, which is $T_d \sim 20$ K (Sodroski et al. 1994). As discussed in Section 3 of Paper I and illustrated in Figures 11, 18, 23, and 26 of Paper I, the molecular gas sampled by the ^{12}CO $J = 1 \rightarrow 0$ line does not fill the beam within each velocity interval within the line profile, especially if the linear beam size at the source is parsecs.

2. The gas not completely filling the beam in each velocity interval may better explain the X-factor. The usual explanation given for the $N(H_2)/I(CO)$ factor is some variation of that of Dickman et al. (1986), that molecular clouds are virialized and that the line width indicates cloud mass and, therefore, cloud column density. In fact, in some cases the velocity-widths of a cloud are only weakly correlated with column densities (e.g., see Heyer et al. 1996). Consequently, a better explanation springs from having filling factors less than unity. This will be discussed in a future paper (Wall 2007b).

3. $\Delta T = 0$ constrains proposed explanations of the dust grain alignment that has been observed in the ISM (Hiltner 1949; Hall 1949). For example, the Davis-Greenstein mechanism is the relaxation of paramagnetic grains spinning in a magnetic field (Davis & Greenstein 1951). This relaxation mechanism requires that $T_d \neq T_{\text{K}}$ (Jones & Spitzer 1967). However, there are number of other possible mechanisms that could explain dust grain alignment that require *no* such difference in temperatures (e.g., see Lazarian et al. 1997; Abbas et al. 2004, and references therein).

Therefore, having equal gas and dust temperatures has a number of interesting consequences that are not *necessarily* contradicted by theory or observations.

4.5. Cold Gas/Dust

The two-component masses compared with those for the one-component masses in Table 6 of Paper I imply about 60% more mass of gas and dust in the Galaxy than previous estimates suggest. These estimates are on the order of $5 \times 10^9 \, \mathrm{M}_\odot$ of gas (i.e. molecular and atomic) in the Galaxy (Dame 1993; Sanders 1993). If the model results for Orion are taken at face value and if these results apply to other clouds throughout the Galaxy, then this total gas mass increases to about $8 \times 10^9 \, \mathrm{M}_\odot$. This increase is due to some positions in component 1 having temperatures below $10 \, \mathrm{K}$ and as low as about $3 \, \mathrm{K}$, nearly that of the cosmic background. Such cold dust and gas emits only weakly per unit mass, allowing much gas and dust to be "hidden" for the observed brightness. Indeed, Table 7 of Paper I lists the cold gas mass and it is about 40% of the total mass listed in Table 6 of Paper I (adopting Case 4 as the more realistic of the two listed in Table 7 of Paper I). Accordingly, the total gas mass is the warm gas mass increased by about 60% to allow for the cold gas mass. Such an increase, especially if it applies to the entire ISM of the Galaxy, is substantial and its validity must be examined carefully.

As mentioned in Section 3.6 of Paper I, the existence of this cold dust and gas depends on the basic assumption used in the modeling. Even if this assumption has provided a good physical description for most of the points in the r_{240} versus T_{dc} plots (e.g., see Figures 20 and 24 of Paper I), it does not necessarily apply to *all* of the triangular cluster of points from $T_{dc} \simeq 15$ to $21 \, \mathrm{K}$ and $r_{240} \simeq 10$ to $70 \, \mathrm{MJy \cdot sr^{-1} \cdot (K \cdot km \cdot s^{-1})^{-1}}$, especially to those with $r_{240} \geq 30 \, \mathrm{MJy \cdot sr^{-1} \cdot (K \cdot km \cdot s^{-1})^{-1}}$. Indeed, it is the $r_{240} \gtrsim 30 \, \mathrm{MJy \cdot sr^{-1} \cdot (K \cdot km \cdot s^{-1})^{-1}}$, $T_{dc} = 18 \, \mathrm{K}$ points that require T_d as low as $3 \, \mathrm{K}$ when the basic assumption applies. If these high-r_{240}, $T_{dc} = 18 \, \mathrm{K}$ points are explained by other means, then such cold gas and dust may not be present. In other words, let us abandon, for the moment, all models that use any form of the basic assumption, at least for these points. There then exist a number of possibilities for the high-r_{240}, $T_{dc} = 18 \, \mathrm{K}$ points:

- The $N(^{13}CO)/\Delta v$ or $n(H_2)$ is different from those of the rest of the points. Models with $N(^{13}CO)/\Delta v$ or $n(H_2)$ that vary smoothly with T_{dc} were discussed in Subsection 3.4. Even though such models have more difficulties than models using the basic assumption, it does *not* exclude this possibility. The $N(^{13}CO)/\Delta v$ value would be higher or the $n(H_2)$ value would be lower. As we saw in Subsection 3.4, $n(H_2)$ would be as low as about $10 \, \mathrm{cm^{-3}}$. Figure 29 of Paper I shows that these points occur mostly on some

edges of the Orion clouds. A lower density for these points is consistent with them being on the cloud edges. However, such low densities imply a peak $T_R(^{13}CO\ J = 1 \rightarrow 0)$ either barely as strong as, or as much as an order of magnitude weaker than, the observed $^{13}CO\ J = 1 \rightarrow 0$ line strength. The other possibility of higher $N(^{13}CO)/\Delta v$ would indeed give strong $^{13}CO\ J = 1 \rightarrow 0$ emission, but implies $N(^{13}CO)/\Delta v$ on the cloud edges a factor of a few higher than that for the cloud central regions. This is possible because $N(^{13}CO)/\Delta v$ is not equivalent to $N(H_2)$, but still seems somewhat implausible.

- The points with high r_{240} values at $T_{dc} \simeq 18\,K$ have appreciable emission of dust associated with atomic hydrogen. Given that this gas is largely found at some cloud edges, this explanation seems reasonable; the atomic hydrogen and its associated dust would be found on molecular cloud edges, thereby providing the shielding necessary for the existence of the molecular gas. However, we examined this in Subsection 3.2 and found, based on the current data, that such emission was not likely to be important. The H I-associated dust contributes negligibly to the observed r_{240} values. Nonetheless, as discussed in that section, the gas and dust of component 1 with temperatures between 3 and 5 K might still be explained by H I-associated dust.

- The ΔT is different for the high-r_{240}, $T_d = 18\,K$ points. Figure 7 of Paper I illustrates that ΔT varying smoothly from 0 to less than $-16\,K$ (e.g., $\simeq -20\,K$) could account for the vertical extent of the points at $T_d = 18\,K$ in the r_{240} versus T_d plot. However, Figure 17 of W96 suggests that G_o is only a few and this would give ΔT less extreme than those of Mochizuki & Nakagawa (2000), rendering $\Delta T \simeq -16$ to $-20\,K$ unlikely. Figure 7 of Paper I also suggests that $\Delta T = +14\,K$ for these points could also account for their vertical extent. But again, this is too extreme for the given G_o. Also, this ΔT combined with $T_d = 18\,K$ would still result in cold gas, $T_K = 4\,K$. A distinct ΔT for these points is an unlikely explanation for their high r_{240} ratio.

- The optical depth of the $^{13}CO\ J = 1 \rightarrow 0$ line is high for these points, while T_K is still well above 3 K. This allows r_{240} to be high, while obviating the need for cold gas. Given that the models require component 1 to be cold for these points (i.e., $T_K = 3$ to 10 K) and component 0 to be 18 K, then the models already require at least some of this gas to be optically thick in the $^{13}CO\ J = 1 \rightarrow 0$ line and some to be optically thin. So, if the observations imply a high $^{13}CO\ J = 1 \rightarrow 0$ optical depth for all of the gas, then the models would be in error. The gas density is near or above the critical density of the $^{13}CO\ J = 1 \rightarrow 0$ transition, so the line is close to LTE. Consequently, the $^{13}CO\ J = 1 \rightarrow 0/^{12}CO\ J = 1 \rightarrow 0$ intensity ratio is a good estimate of the optical depth of $^{13}CO\ J = 1 \rightarrow 0$. This ratio for these points is about 0.3 — significantly less

than unity. Therefore, at least some gas is indeed optically thin in ^{13}CO J $= 1 \rightarrow 0$, in agreement with the models.

- A lower ^{13}CO abundance or a higher dust-to-gas ratio for these points could account for the high r_{240} values. Accordingly, X(^{13}CO) would be factors of 2 to 3 lower or x_d would be similar factors higher. There is no observational evidence for large changes in the ^{13}CO abundance or the dust-to-gas mass ratio. Nevertheless, the models of Warin et al. (1996) suggest that selective photodissociation of ^{13}CO reduces its abundance by factors of 2 or 3 near molecular cloud surfaces. If the triangular cluster of points in the r_{240} versus T_{dc} plot were affected by this reduced X(^{13}CO), then correcting to the "normal" abundance would bring these points down by factors of 2 to 3. This would increase the lower temperature limit of the cold gas. The bend in the model curve from vertical to horizontal occurs more or less at the bottom of the triangular cluster and more or less for a component-1 temperature of 7 K. Consequently, correcting for a *possible* reduced ^{13}CO abundance *could possibly* bring the lower temperature limit up to slightly less than 7 K.

- A similar possibility would be an emissivity enhancement of the dust: the dust mass absorption coefficient, i.e. κ_ν at 240 μm, would be unusually large, by factors of 2 to 3, for these points. For example, a resonance in the dust absorption spectrum at 240 μm could produce an increase in κ_ν at 240 μm. However, an increase by the same factor would be needed at 140 μm in order to maintain T_{dc} at about 18 K. This resonance feature would be at least 100 μm wide. This is very unlikely. Instead of a resonance, dust with opacities 2 to 3 times higher than normal dust at all FIR wavelengths is sufficient. Dwek (2004), for example, discusses dust grains with far-IR opacities orders of magnitudes higher than the classical silicate, graphite grains. Mixing a very small portion of such grains with classical grains could give a mix with an effective far-IR opacity easily factors of 2 to 3 higher than considered here. However, the observations require the opacity to increase as the r_{240} value increases towards the top of the triangular cluster. Increasing opacity at far-IR wavelengths increases cooling as well. Consequently, there would be an obvious overall trend to lower and lower 140 μm/240 μm color temperature as r_{240} increased — resulting in a triangular cluster whose peak would be noticeably skewed towards lower colour temperatures. This is not observed. Increasing the far-IR emissivity while keeping the 140 μm/240 μm color temperature constant requires having another warmer component mixed in that dominates the dust continuum emission. But this is nothing more than the original two-component models that have been used up to this point. Also, grains with such high far-IR emissivities are more likely to be responsible for such low dust temperatures (i.e. about 3 – 5 K) rather than rule them out.

- Yet another possibility is that points towards the peak of the triangular cluster are dominated by a component with a large value of r_{240} and T_{dc} around $18\,K$. In terms of the two-component models discussed in the current work, this is equivalent to increasing the parameter c_0 for the peak of the triangular cluster.

It seems that at least some alternatives to cold dust and gas may exist. Overall, however, the evidence is far from convincing. In addition, simply abandoning the basic assumption leads to ad hoc interpretations. This is probably unjustified given the success of the basic assumption, and its associated models, at accounting for the overall trend in the data; the basic assumption and the models should *not* be so lightly discarded.

Can we explain the data without such cold dust and gas and still use the models and the basic assumption? In other words, is there some unexplored region of parameter space that permits a higher lower limit on the dust and gas temperature of component 1? The answer is yes, but the changes are *not* dramatic. The lower limit to T_{K1} and T_{d1} depends on the position of the "component-0 point". That is, the physical parameters of component 0 are constant in every respect and therefore represent a single point in the r_{240} versus T_{dc} plot. In contrast, the gas and dust temperatures of component 1 vary spatially, while the other parameters are held constant, and therefore the parameters of component 1 represent a locus of points in this plot. The position of the component-0 point is just above the vertical section of the plotted two-component model curve. When the r_{240} of the component-0 point is higher than the apex of the triangular cluster, then the lower limit on T_{d1} is higher. In fact, this lower limit is roughly given by T_{d1} on the model curve at the apex position. Hence, the relevant parameter space area is where the component-0 point has higher r_{240}. This is easily accomplished by reducing the ^{13}CO abundance *of component 0 only* by a factor of 2. Doing this, and refitting the two-component models, raises the component-0 point from $r_{240} \simeq 65$ to about $110\,MJy \cdot sr^{-1} \cdot (K \cdot km \cdot s^{-1})^{-1}$. However, simply keeping the ^{13}CO abundance fixed at its usual value and restricting c_o to be ≥ 1 results in even higher r_{240} for the component-0 point. In spite of the more promising position of this point, T_{d1} at the apex of the triangular cluster changes only by about $0.5\,K$. If we truncate the model curve above the $T_{d1} = 5\,K$ point (i.e. remove the temperatures *lower* than this), and keeping $\Delta T \geq 0\,K$ to keep $T_{K1} \geq 5\,K$ as well, then the χ_ν^2 increases from 5.6 to 8.1, an increase excluded by the F-test at a confidence level of more than 90%. Accordingly, raising the component-0 point to higher r_{240} merely stretches the vertical section of the curve between $T_{d1} = 2.8\,K$ and $T_{d1} \simeq 5\,K$. Consequently, we only increase the lower limit on T_{d1} from about $3\,K$ to about $3.5\,K$. In short, there is no compelling evidence that rules out cold dust and gas.

Previous evidence for cold dust or gas is not compelling either, but does nonetheless come from a wide variety of observations (e.g., Reach et al. 1995; Merluzzi et al. 1994;

Ristorcelli et al. 1998). In addition, there is evidence for gas that had been previously unde-tected (e.g., Reach et al. 1998; Cuillandre et al. 2001). Reach et al. (1995) used *COBE/FIRAS* continuum data with observed wavelengths from $104\,\mu$m to $2\,$mm to infer a widespread cold component with dust temperatures 4 to $7\,$K. This component is found at all Galactic lati-tudes from the Galactic plane to the Galactic poles. Lagache et al. (1998) re-examined the *FIRAS* data and concluded that the cold component of Reach et al. (1995) was not needed; the coldest component necessary was at about $15\,$K. Finkbeiner et al. (1999), in yet another examination of the FIRAS data, concluded that the colder component has a temperature of about $9\,$K. Merluzzi et al. (1994) found a cold component with a temperature of either $15\,$K or $7\,$K, depending on whether the spectral emissivity index, β, was 1.1 or 2, respec-tively. Ristorcelli et al. (1998) armed with continuum observations in four wavelength bands (i.e., 180-240, 240-340, 340-560, 560-1050 μm) discovered a "cold condensation" close to the Orion Nebula with a temperature of $12.5\pm3\,$K. This is not as cold as the 3 to $10\,$K material discussed here, but nevertheless shows that dust with temperatures significantly lower than the $18\,$K expected for dust heated primarily by the general ISRF is possible. In contrast to these previous papers, the current paper infers a cold component (i.e. T$\simeq 3$ to $10\,$K) with*out* benefit of long-wavelength (i.e. $\lambda \gtrsim 1\,$mm) *continuum* data. The long-wavelength data used here is the $2.7\,$mm ^{13}CO J $= 1 \to 0$ *spectral line* in emission.

If we accept for the moment that a cold component with temperatures of 3 to $10\,$K does indeed exist within the Orion clouds, then the obvious question is how can such cold gas and dust exist without being strongly affected by the general ISRF or local stars? Reach et al. (1995) discuss a number of possible explanations in the context of cold dust throughout the Galaxy, especially in high-latitude clouds. We revisit some of the proposed explanations of Reach et al. (1995), but in the context of the Orion clouds:

Shielding from the Interstellar Radiation Field. As Reach et al. (1995) point out, atten-uating the heating rate by a factor of 10^3 requires a *minimum* absorption equivalent to $A_v = 20\,mag$ (Mathis et al. 1983). Given that the radiation field is proportional to T_d^6 and that $T_d = 3$ to $10\,$K is the cold dust temperature range, then attenuation factors of roughly 30 to 5×10^4 are necessary. This then requires minimum absorptions equivalent to $A_v \simeq few\,mag$ to A_v considerably more than $20\,mag$ (Mathis et al. 1983). These correspond to column densities of a $few \times 10^{21}$ to more than 3×10^{22} $H\ nuclei$·cm^{-2}. Over much of their area, the Orion clouds have N(H) closer to the former value. Con-sequently, shielding might explain the $T_d = 10\,$K material, but is unlikely to explain the really cold material ($T_d \sim 5\,$K). Also, since most of this cold material is on the cloud edges, shielding probably will not account for the cold dust and gas suggested by the models.

Fractal Grains. As previously mentioned, grains with enhanced submillimeter/FIR emission relative to UV/visible absorption, like the iron needles discussed by Dwek (2004) or fractal grains (see Reach et al. 1995, and references therein), can have temperatures near that of the cosmic background. Reach et al. (1995) state that fractal grains may have greatly reduced mass for the given absorption cross-section; the 60% upward correction to the single-component mass would be revised considerably downward. In addition, fractal grains may also have a reduced volume for the given geometric cross-section, permitting $\Delta T \simeq 0$, as discussed previously (see also Appendix A).

Very Large Grains. Dust grains larger than the FIR wavelengths that they emit do so very efficiently and, therefore, cool very efficiently. Reach et al. (1995) find that the size distribution of these grains must steepen beyond that of the power-law index of -3.5 of Mathis et al. (1977) to explain their observations. This steepening prevents a dust-to-gas mass ratio much higher than observed; the power-law index of -3.5 out to a maximum grain radius of $100\,\mu$m increases the dust-to-gas mass ratio by more than an order of magnitude. In addition, the current work requires the observed grains to have a large geometric cross-section to volume ratio, thereby ruling out such large grains being the bulk of the cold dust.

Long-Wavelength Emissivity Enhancement. Reach et al. (1995) suggest that an enhancement of the continuum emissivity at $\lambda \simeq 800\,\mu$m could explain their observations instead of some hypothetical cold dust. Obviously, this explanation does not apply to the current paper because the models have been applied to $240\,\mu$m continuum data and $2.7\,$mm *spectral line* data. If the cold material predicted by the models for the Orion clouds is indeed ubiquitous in the Galaxy, then the Reach et al. (1995) proposed enhancement of the long-wavelength continuum emissivity cannot rule it out.

Of the explanations given above, fractal grains may be the most feasible.

Thus the observations neither completely exclude nor strongly support the existence of cold dust and gas (i.e. T$\simeq 3$ to $10\,$K) in the Orion clouds nor a widespread presence in the Galaxy as a whole. The least unlikely alternative to dust and gas at temperatures of 3–5 K is probably that mentioned in Subsection 3.2: the additional emission of dust grains associated with atomic hydrogen. Nevertheless, it seems likely that cold material with temperatures of 7 to $10\,$K does exist in the Orion clouds. If cold dust and gas exist in the ISM in general with temperatures of ~ 3 to $10\,$K, then fractal dust grains or iron needles may be the most credible reason and the 60% upward correction to the Galactic ISM's mass due to this cold material might be revised downward substantially. This downward revision is also necessary if the material at temperatures of 3 to $7\,$K is really an artefact due to the other effects just described.

4.6. The Millimeter Continuum to ^{13}CO J $= 1 \rightarrow 0$ Ratio as a Temperature Diagnostic

Given that we can now characterize the $I_\nu(240\,\mu\text{m})/I(^{13}\text{CO J} = 1 \rightarrow 0)$ ratio as a function of physical parameters like the temperature, continuum and ^{13}CO J $= 1 \rightarrow 0$ observations can constrain the temperature of the dust and molecular gas. In particular, using only ground-based observations to achieve such a constraint is advantageous. Consequently, we examine one particular representative case: using the $I(1300\,\mu\text{m})/I(^{13}\text{CO J} = 1 \rightarrow 0)$ ratio — hereafter, r_{1300} — to estimate the dust temperature, T_d.

To this end, the simulations described previously in Paper II were used to generate a model $1300\,\mu\text{m}$ continuum map. The adopted mass absorption coefficient at $1300\,\mu\text{m}$, $\kappa_\nu(1300\,\mu\text{m})$, was determined from the adopted $\kappa_\nu(100\,\mu\text{m})$ of $40\,\text{cm}^2 \cdot \text{g}^{-1}$ and scaling by ν^β for $\beta = 2$, yielding $\kappa_\nu(1300\,\mu\text{m}) = 40\,\text{cm}^2 \cdot \text{g}^{-1} \times (100/1300)^2$ or $0.24\,\text{cm}^2 \cdot \text{g}^{-1}$. To adopt a reasonable noise level, we note that current bolometers can achieve an rms noise value of $2\,\text{MJy} \cdot \text{sr}^{-1}$ for a 1-hour integration in a $15''$ beam at wavelength of $450\,\mu\text{m}$ (D. Hughes, priv. comm.). Assuming a noise proportional to λ^{-2} and, depending on the integration time and spatial averaging of the observations, a noise level of $0.075\,\text{MJy} \cdot \text{sr}^{-1}$ at $1300\,\mu\text{m}$ is possible. Therefore, this rms noise level is adopted for the simulated $1300\,\mu\text{m}$ map. The simulated $1300\,\mu\text{m}$ continuum map was divided by the simulated ^{13}CO J $= 1 \rightarrow 0$ map to produce the r_{1300} map. Figure 4 shows the resultant simulated r_{1300} values plotted against the simulated T_dc values — the $140\,\mu\text{m}/240\,\mu\text{m}$ color temperature. This color temperature is, of course, not directly relevant to $1300\,\mu\text{m}$ observations, but is included in Figure 4 to permit easy comparison with the standard r_{240} versus T_dc plots used throughout the current paper.

The upper panel of Figure 4 shows that r_{1300} is *not* useful as a temperature diagnostic for dust *color* temperatures of ~ 15 to $30\,\text{K}$; given that the vertical spread of the data points is about the size of the vertical error bars, we cannot unambiguously associate each r_{1300} with a single T_dc. The temperature dependence is weak in this range, because both the continuum and line observations are close to the Rayleigh-Jeans limit. This implies that neither component's emission will overwhelmingly dominate over the other's for a larger range of temperature differences between the two components. In contrast, at $\lambda = 240\,\mu\text{m}$ and in the ~ 3 to $30\,\text{K}$ range of dust *physical* temperatures, component 1 goes from being overwhelmingly dominated by to overwhelmingly dominating the component-0 emission. At $\lambda = 1.3\,\text{mm}$, component-1 goes from being dominated by only factors of a few to dominating by only a factor of ~ 2. Accordingly, combined emission of the two components has a narrow range of brightnesses.

In contrast, the lower panel of Figure 4 demonstates that r_{1300} can indeed be a temperature diagnostic. This plot shows the model curve up to temperatures of $200\,\text{K}$, and the

simulated map data points in the lower left corner. The curve goes from nearly flat (i.e. slope near 0) for $T_{dc} \simeq 15$ to $30\,K$ to a power law with

$$r_{1300} \propto T_d^{1.4} \tag{3}$$

above a threshold of

$$r_{1300} \gtrsim 0.5\,\mathrm{MJy} \cdot \mathrm{sr}^{-1} \cdot (\mathrm{K} \cdot \mathrm{km} \cdot \mathrm{s}^{-1})^{-1} \quad \mathrm{and} \quad T_d \gtrsim 50\,\mathrm{K} \qquad . \tag{4}$$

(Note that T_d can serve in place of T_{dc} for high temperatures, because the effect of component 0 is negligible in this limit.) Therefore, r_{1300} is a useful temperature diagnostic for temperatures above about $50\,K$ or r_{1300} above $\sim 0.5\,\mathrm{MJy} \cdot \mathrm{sr}^{-1} \cdot (\mathrm{K} \cdot \mathrm{km} \cdot \mathrm{s}^{-1})^{-1}$. Also, above this threshold the temperature sensitivity increases with increasing temperature. This is not quite as strong as the T_d^2 rise expected in the LTE, high-temperature limit, but is definitely much better high-temperature sensitivity than for the ratio of two rotational lines of CO or for the ratio of two continuum bands.

Naturally, the real situation is considerably more complicated than simply reading the temperature from this one curve that *may* apply *only* to the Orion clouds. As we recall, there are a number of physical parameters that affect this curve: T_{d0}, $\frac{N_{c0}}{\Delta v_c}$, c_0, n_{c0}, $\frac{N_{c1}}{\Delta v_c}$, n_{c1}, ΔT, κ_ν (or β), x_d, and $N(H\,I)/N(H_2)$. Before we examine how variations of these parameters effect the model curve, the curve in Figure 4 is adopted as the nominal curve. The T_d inferred from an observed r_{1300} using this nominal curve we call the nominal T_d. Then the question is how the true T_d differs from the nominal T_d due to physical parameters differing from their nominal values (see the "Input Values" column of Table 1 of Paper II). A reasonable goal is a temperature estimate within a factor of 2 of the true temperature for those "hot spots" where r_{1300} is above the threshold value of $0.5\,\mathrm{MJy} \cdot \mathrm{sr}^{-1} \cdot (\mathrm{K} \cdot \mathrm{km} \cdot \mathrm{s}^{-1})^{-1}$. If we vary the component-0 parameter values (i.e. the first four parameters listed above), then the true T_d stays within a factor of 2 of the nominal T_d in most cases. Specifically, varying T_{d0} from values lower than nominal to double this, $c_0 \frac{N_{c0}}{\Delta v_c}$ from factors 10 or more lower (since this represents the optically thin limit), and n_{c0} from $10\,\mathrm{cm}^{-3}$ to $10^5\,\mathrm{cm}^{-3}$ and higher (since this represents the LTE limit) changes r_{1300} by only 5-7%. Equivalently, the true T_d differs from the nominal value by 7-10%, well within the desired factor of 2. There are two potential difficulties. One is if $c_0 \frac{N_{c0}}{\Delta v_c}$ is two orders of magnitude higher than the nominal value, then the true r_{1300} is 80% lower than its nominal value. In practice this would not be a problem because the observed r_{1300} would be low enough that this observed position would not be identified as a hot spot; there would be no false positives in the search for hot spots. Nevertheless, any false hot spot is easily identifiable with supplemental observations of the $J = 1 \rightarrow 0$ line of $C^{18}O$ or ^{12}CO; the $C^{18}O/^{13}CO$ intensity ratio would identify the position as having high $^{13}CO\ J = 1 \rightarrow 0$ opacity. The $^{13}CO/^{12}CO$ intensity ratio could be used similarly, but $C^{18}O/^{13}CO$ would be

more reliable given that the corresponding abundance ratio is within an order of magnitude of unity. Another potential difficulty is that, even though varying n_{c0} over many orders of magnitude has a negligible effect on r_{1300} for $T_{dc} \geq 50\,K$, n_{c0} as low as $10\,cm^{-3}$ can raise the spur of data points at $T_{dc} \simeq 18\,K$ (see Figure 4) by about 70%. Accordingly, the threshold listed above, expressions (4), is raised to

$$r_{1300} \gtrsim 0.85\,MJy \cdot sr^{-1} \cdot (K \cdot km \cdot s^{-1})^{-1} \quad \text{and} \quad T_d \gtrsim 60\,K \qquad . \tag{5}$$

Densities as low as $10\,cm^{-3}$ are probably unlikely, so threshold (5) is probably unnecessary. Nevertheless, it can be used if extra caution is desired.

Varying the component-1 parameters $\frac{N_{c1}}{\Delta v_c}$ and n_{c1} results in the true T_d being up to a factor of 5 smaller than the nominal T_d. The $\frac{N_{c1}}{\Delta v_c}$ value was increased by an order of magnitude or decreased similarly (or more because this is the optically thin limit). At the same time, the n_{c1} value was decreased to $100\,cm^{-3}$ (again assuming that densities as low as $10\,cm^{-3}$ are unlikely) and increased to $10^5\,cm^{-3}$ (or more because this is the LTE limit). Over most of this parameter space the true T_d stayed within a factor of 2 of the nominal T_d. However, the combination of n_{c1} as low as $100\,cm^{-3}$ and $\frac{N_{c1}}{\Delta v_c}$ an order of magnitude larger gives a true T_d up to a factor of 5 smaller than the nominal T_d. This low temperature case can be identified by observing the $^{13}CO\ J = 2 \rightarrow 1$ line. In the nominal case, the ratio $I(^{13}CO\ J = 2 \rightarrow 1)/I(^{13}CO\ J = 1 \rightarrow 0)$ varies between 1.9 and 3.4 for $T_K = 50$ to $200\,K$. In this high-$\frac{N_{c1}}{\Delta v_c}$, low-$n_{c1}$ case, $I(^{13}CO\ J = 2 \rightarrow 1)/I(^{13}CO\ J = 1 \rightarrow 0)$ is 0.5 to 0.7. Supplemental continuum observations help as well. The $I_\nu(450\,\mu m)/I_\nu(1300\,\mu m)$ ratio, for example, is sensitive to temperatures up to $T_d \simeq 60\,K$ for a flux ratio uncertainty of 20%. Consequently, the observed $I_\nu(450\,\mu m)/I_\nu(1300\,\mu m)$ ratio places a lower limit on T_d.

Considering variations in ΔT, the determination of T_d is remarkably insensitive to such variations. For example, ΔT could range from $-80\,K$ to $+80\,K$ and the true T_d is still within about 20% of the nominal T_d. Of course, the T_K would be quite different from T_d in that case. For $\Delta T = -80\,K$, the T_K is even higher than a nominal T_d that was already high; this T_K is still within a factor of roughly 2 of the nominal T_d. For $\Delta T = +80\,K$, T_K is quite small. The $I(^{13}CO\ J = 2 \rightarrow 1)/I(^{13}CO\ J = 1 \rightarrow 0)$ ratio is low in this case, but it is difficult to distinguish this case from the low-T_d, low-density case described in the previous paragraph using only this CO-line ratio. Using the $I_\nu(450\,\mu m)/I_\nu(1300\,\mu m)$ ratio in conjunction with the $I(^{13}CO\ J = 2 \rightarrow 1)/I(^{13}CO\ J = 1 \rightarrow 0)$ may provide sufficient information to distinguish this high-T_d, low-T_K case from the low-T_d, low-density case.

Dealing with anomalous values of the remaining parameters — κ_ν (or β), x_d, and $N(H\,I)/N(H_2)$ — is problematic but still possible. If a source (a molecular cloud or part of another galaxy) is mapped in $I_\nu(1300\,\mu m)$ and $^{13}CO\ J = 1 \rightarrow 0$, then the majority of the positions probably have roughly constant values for these parameters; the majority of these

positions would also have similar values of r_{1300}. For example, it is easy to imagine that the molecular clouds in another galaxy have an unusually high or low dust-to-gas ratio, i.e. high or low x_d, compared with such clouds in our Galaxy. Or we can imagine a cloud that has a non-negligible layer of atomic gas (i.e. non-negligible $N(H\,I)/N(H_2)$). In cases such as these, the r_{1300} value itself would not be important, but that value in relation to the "average" r_{1300} values for the observed source. The hot spots are identified as those with r_{1300} values large compared to the typical value for the source. If, instead, such hot spots are not due to elevated temperatures but unusual κ_ν, x_d, and/or $N(H\,I)/N(H_2)$ values, then such "hot spots" would *still* be interesting: they represent positions with unusual properties. Specifically identifying those unusual properties would involve the supplemental observations described above — using the $I(^{13}CO\ J = 2 \rightarrow 1)/I(^{13}CO\ J = 1 \rightarrow 0)$ and $I_\nu(450\,\mu m)/I_\nu(1300\,\mu m)$ ratios — and other observations when possible.

Addressing the various points mentioned above, the following is a plausible observing plan:

1. First map the $1300\,\mu m$ continuum and the $^{13}CO\ J = 1 \rightarrow 0$ line. The majority of points establish the typical r_{1300} value for the source. Any points with high r_{1300} values, above some threshold that applies to the source, would be hot spots to be ear-marked for further observations and study. The r_{1300} values for these hot spots will provide a temperature estimate to within a factor of 2 in the majority of cases.

2. Map the $^{13}CO\ J = 2 \rightarrow 1$ line. The $I(^{13}CO\ J = 2 \rightarrow 1)/I(^{13}CO\ J = 1 \rightarrow 0)$ ratio can help confirm whether the hot spots are indeed hot.

3. Map the $450\,\mu m$ (or shorter) continuum. The $I_\nu(450\,\mu m)/I_\nu(1300\,\mu m)$ ratio is a further check on the temperature and can, in some cases, check whether $\Delta T = 0$ or not.

4. Map the $C^{18}O\ J = 1 \rightarrow 0$ line. The $I(C^{18}O\ J = 1 \rightarrow 0)/I(^{13}CO\ J = 1 \rightarrow 0)$ ratio can confirm that $^{13}CO\ J = 1 \rightarrow 0$ is indeed optically thin, thereby further checking the temperature inferred from the r_{1300} of the hot spots. Even though the $^{13}CO\ J = 1 \rightarrow 0$ is expected to be optically thin on multi-parsec scales, as in the Orion clouds, verification of this can rule out other possibilities.

All of these observations are possible from the ground.

Obviously, this is only one proposed observing plan out of many possibilities. Similar plans could be devised using other continuum wavelengths and other rotational lines. Two such alternatives would be the $I_\nu(2700\,\mu m)/I(^{13}CO\ J = 1 \rightarrow 0)$ ratio or the $I_\nu(1300\,\mu m)/I(^{13}CO\ J = 2 \rightarrow 1)$ ratio. This is re-discovering the line-to-continuum (similarly, the continuum-to-line) ratio or the equivalent width, but for millimeter- or

submillimeter-wave molecular lines. Such equivalent widths are commonly used at visible, infrared, and centimeter wavelengths for inferring the physical properties of H II regions (Osterbrock 1989; Spitzer 1978). Likewise, the equivalent widths of millimeter-wave molecular lines can provide important physical insights into molecular clouds (i.e. H_2 regions).

Nevertheless, the ^{13}CO $J = 1 \rightarrow 0$ line has a big advantage over higher rotational lines of ^{13}CO: *relative* insensitivity to physical parameters like density and column density per velocity interval. This is why the r_{1300} ratio can often predict T_d to within a factor of 2, *despite varying* $n(H_2)$ *and* $N(^{13}CO)/\Delta v$ *by orders of magnitude.* At the very least, this method potentially places a realistic and interesting upper limit on dust and molecular gas temperatures.

5.   Conclusions

Far-infrared continuum data from the *DIRBE* instrument aboard the *COBE* spacecraft were combined with ^{13}CO $J = 1 \rightarrow 0$ spectral line data from the Nagoya 4-m telescope to infer the large-scale (i.e. ~ 5 to $\sim 100\,pc$) physical conditions in the Orion molecular clouds. The $140\,\mu m/240\,\mu m$ dust color temperatures, T_{dc}, were compared with the $240\,\mu m/^{13}CO$ $J = 1 \rightarrow 0$ intensity ratios, r_{240}, to constrain dust and molecular gas physical conditions. In addition, such a comparison provides valuable insights into how the ratio of FIR/submillimeter/millimeter continuum to that of a ^{13}CO (or $C^{18}O$) rotational line can constrain temperature estimates of the dust and molecular gas. For example, ratios of rotational lines or ratios of continuum emission in different wavelength bands often cannot place realistic upper limits on gas or dust temperature, whereas the continuum-to-line ratio can place such limits.

Two-component models fit the Orion data best. One component has a fixed-temperature and represents the gas and dust towards the surface of the clouds and is heated primarily by a kiloparsec-scale interstellar radiation field, referred to here as the general ISRF. The other component has a spatially varying temperature and represents gas and dust towards the interior of the clouds that can be both shielded from the general ISRF and heated by local stars. The model results and their implications are as follows:

1) The inferred physical conditions are consistent with those derived from the large-scale observations of the $J = 2 \rightarrow 1$ and $J = 1 \rightarrow 0$ lines of ^{12}CO by Sakamoto et al. (1994).

2) At least two gas (dust) temperatures are needed on the majority of sightlines through molecular clouds for reliably estimating column densities. This is supported by the work of Schnee et al. (2006).

3) The dust-gas temperature difference, $T_d - T_K$ or ΔT, is 0 K to within 1 or 2 K. If this result applies more generally to the Galactic-scale molecular ISM, except for unusual regions such as the Galactic Center, then there are a number of implications:

- Dust-gas thermal coupling is factors of 5 to 10 stronger than has been previously assumed. Such factors may be due to the distribution of dust grain sizes and grains with larger cross-section to volume ratios than that of a simple sphere.

- Galactic-scale molecular gas temperatures are closer to 20 K than to 10 K, because the emission from the CO rotational lines, even the optically thick ^{12}CO J $= 1 \rightarrow 0$ line, does not fill the beam within the velocity interval about the line peak.

- This CO emission that does not fill the beam provides a better explanation of the $N(H_2)/I(CO)$ conversion factor or X-factor. Discussion of this is deferred to a later paper (Wall 2007b).

- Having ΔT nearly 0 constrains which mechanisms explain dust grain alignment in the ISM. A negligible dust-gas temperature difference rules out the Davis-Greenstein alignment mechanism, but not other possible mechanisms (see Lazarian et al. 1997; Abbas et al. 2004, and references therein).

4) Roughly 40–50% of the ISM in Orion is cold (i.e. 10 K) to very cold (i.e. down to 3 K) dust and gas. Accordingly, there is roughly 60% more gas and dust in Orion than inferred from simple one-component models. This *may* also imply a similar increase in the estimated mass of entire Galactic ISM. Fractal dust grains (see Reach et al. 1995, and references therein) or iron needles (Dwek 2004) may explain the low temperatures of this gas and dust and, at the same time, may account for the high dust-gas thermal coupling needed to explain $\Delta T \simeq 0$ K. Nevertheless, alternative explanations that do *not* require cold dust and gas cannot be ruled out; the least unlikely of these other explanations is a contribution to the 240 μm continuum emission of the dust associated with atomic hydrogen. The data suggest that the effect of the H I-associated dust is negligible, but still might permit raising the lower temperature limit of this cold gas and dust from 3 to 5 K.

The model parameter values derived from the fits to the r_{240} versus T_{dc} plots were used to create simulated 1300 μm continuum and ^{13}CO J $= 1 \rightarrow 0$ line maps. These simulated maps tested whether the millimeter continuum to ^{13}CO J $= 1 \rightarrow 0$ line intensity ratio could constrain temperature estimates of the dust and molecular gas. The ratio $I_\nu(1300\,\mu\text{m})/I(^{13}\text{CO J} = 1 \rightarrow 0)$, or r_{1300}, was found to estimate the dust temperature to within a factor of 2 in most cases, provided that r_{1300} was higher than a threshold level of $0.5\,\text{MJy} \cdot \text{sr}^{-1} \cdot (\text{K} \cdot \text{km} \cdot \text{s}^{-1})^{-1}$. Supplemental observations of the ^{13}CO J $= 2 \rightarrow 1$ line and

shorter wavelength continuum would confirm the high temperatures in these high-r_{1300} "hot spots". The results here can be easily generalized to other continuum wavelengths and other rotational lines, even permitting interpretation of millimeter and submillimeter molecular line *equivalent widths.* And this is entirely possible with only ground-based observations.

The full potential of using millimeter continuum and ^{13}CO (or C^{18}O) rotational line comparisons has yet to be realized.

A.   The Effect of Grain Size on Gas-Grain Thermal Coupling

Burke & Hollenbach (1983) describe the heat transfer rate from the gas to the dust (or vice versa) as

$$\Lambda_{\rm gd} = n_{\rm H2} n_{\rm gr} \sigma_{\rm gr} \left(\frac{8kT_{\rm K}}{\pi m_{\rm H2}}\right)^{\frac{1}{2}} \bar{\alpha}_{\rm T}(2k)(T_{\rm K} - T_{\rm d}) \qquad , \tag{A1}$$

where $n_{\rm H2}$ and $n_{\rm gr}$ are the number densities of hydrogen molecules and dust grains, respectively, $\sigma_{\rm gr}$ is the grain *geometric* cross-sectional area, $T_{\rm K}$ is the gas kinetic temperature, $T_{\rm d}$ is the dust grain temperature, $m_{\rm H2}$ is the mass of the hydrogen molecule, and $\bar{\alpha}_T$ is the accommodation coefficient. This coefficient is a measure of how well the temperature of the gas particles that have collided with the dust grains accommodate to that of the grain surface (Burke & Hollenbach 1983). (Note that the $n_{\rm H2}$ and $m_{\rm H2}$ in this expression replace the $n_{\rm H}$ and $m_{\rm H}$ in expression 9 of Burke & Hollenbach (1983) because the colliders considered here are hydrogen molecules.) If we simplistically assume identical grains, then

$$x_d = \frac{n_{\rm gr} m_{\rm gr}}{n_{\rm H2} m_{\rm H2}} \tag{A2}$$

or

$$n_{\rm gr} = \frac{x_d n_{\rm H2} m_{\rm H2}}{m_{\rm gr}} \qquad , \tag{A3}$$

where m_{gr} is the mass of a single dust grain. Assuming spherical grains of uniform density, ρ_{gr}, yields

$$m_{gr} = \frac{4}{3}\pi a^3 \rho_{gr} \tag{A4}$$

and

$$\sigma_{gr} = \pi a^2 \quad , \tag{A5}$$

where a is the grain radius. Expression (A4) substituted into (A3) gives

$$n_{gr} = \frac{3}{4}\frac{x_d n_{H2} m_{H2}}{\pi a^3 \rho_{gr}} \tag{A6}$$

and multiplying the above by (A5) yields

$$n_{gr}\sigma_{gr} = \frac{3}{4}\frac{x_d n_{H2} m_{H2}}{a \rho_{gr}} \quad . \tag{A7}$$

Note that expression (A7) is nearly identical to expression (5) of Goldsmith (2001); he also included a Q-correction factor that is not necessary here because we are only concerned with the geometric cross-section and not the absorption cross-section. Note also that (A7) is proportional to the grain cross-section to volume ratio. (In reality, it is the grain cross-section to mass ratio that is relevant, but, for a uniform grain density, this is equivalent to a proportionality to the cross-section to volume ratio.) Substituting (A7) into (A1) yields

$$\Lambda_{gd} = \frac{3}{2}\left(\frac{8k^3 m_{H2}}{\pi}\right)^{\frac{1}{2}} \bar{\alpha}_T \frac{x_d}{a \rho_{gr}} n_{H2}^2 (T_K - T_d) T_K^{\frac{1}{2}} \quad . \tag{A8}$$

Putting in the physical constants in cgs units gives

$$\Lambda_{gd} = 7.11 \times 10^{-36} \, \bar{\alpha}_T \frac{x_d}{a \rho_{gr}} n_{H2}^2 (T_K - T_d) T_K^{\frac{1}{2}} \quad . \tag{A9}$$

Goldsmith (2001) adopted the following values for the dust parameters: $x_d = 0.01$, $\rho_{gr} = 2\,\text{g} \cdot \text{cm}^{-3}$, and $a = 1.7 \times 10^{-5}\,\text{cm}^{-3}$. [Note that Goldsmith (2001) *apparently* adopted $a = 1.7 \times 10^{-7}\,\text{cm}^{-3}$, but this is near the lower limit of the dust grain size range (see Désert et al. 1990). Also, and more importantly, that value of a is inconsistent with the numerical coefficients in the expressions for Λ_{gd}. Finally, $a = 1.7 \times 10^{-5}\,\text{cm}^{-3}$ was the actual *intended* dust grain radius (Goldsmith, *priv. comm.*).] The recommended value of the accommodation coefficient is $\bar{\alpha}_T = 0.3$ (Burke & Hollenbach 1983). Consequently,

$$\Lambda_{gd} = 2.0 \times 10^{-33}\, n_{H2}^2 (T_K - T_d)\left(\frac{T_K}{10\,\text{K}}\right)^{\frac{1}{2}} \quad , \tag{A10}$$

as per Goldsmith (2001).

However, as stated in Section 4.4, Λ_{gd} must be factors of 5 to 10 larger to explain the observations. This is achieveable using a more realistic treatment of grain sizes in deriving Λ_{gd}. Specifically, a range of grain sizes must be considered instead of simplistically adopting a single radius. For example, Désert et al. (1990) suggest that $a = 15$ to $110\,\mathrm{nm}$ for the big thermal equilibrium grains. Consequently, the $170\,\mathrm{nm}$ adopted by Goldsmith (2001) is clearly too large; instead, some appropriately weighted mean of $15\,\mathrm{nm}$ and $110\,\mathrm{nm}$ is the most realistic choice for the a in expression (A9). From the work of Mathis et al. (1977) we know that

$$\mathrm{n_{gr}}(a) = k_0 a^{-3.5} \quad , \tag{A11}$$

where $\mathrm{n_{gr}}(a)\mathrm{d}a$ is the number density of grains with radii between a and $a + \mathrm{d}a$ and k_0 is a normalizing constant. The k_0 is found from

$$\mathrm{n_{gr}}(\mathrm{tot}) = k_0 \int_{a_{min}}^{a_{max}} a^{-3.5}\, da \quad , \tag{A12}$$

with $\mathrm{n_{gr}}(\mathrm{tot})$ as the number density of all the grains and corresponds to the $\mathrm{n_{gr}}$ in (A2) and (A3). From (A12), k_0 can be expressed as

$$k_0 = \mathrm{n_{gr}}(\mathrm{tot})\, k_1 \quad . \tag{A13}$$

k_1 is another constant of the distribution and depends on a_{min} and a_{max}. Its exact form is not relevant to the derivation here, but is nonetheless given below for completeness:

$$k_1 = 2.5\, \frac{(a_{min} a_{max})^{2.5}}{a_{max}^{2.5} - a_{min}^{2.5}} \quad . \tag{A14}$$

To include the effect of the range of grain sizes on Λ_{gd}, the $\mathrm{n_{gr}}\sigma_{\mathrm{gr}}$ in equation (A1) must be replaced with $\mathrm{n_{gr}}(\mathrm{tot})\langle\sigma_{\mathrm{gr}}(a)\rangle_a$, where $\langle\sigma_{\mathrm{gr}}(a)\rangle_a$ is the grain cross-section after averaging over the size distribution. Thus,

$$\mathrm{n_{gr}}(\mathrm{tot})\langle\sigma_{\mathrm{gr}}(a)\rangle_a = \int_{a_{min}}^{a_{max}} \mathrm{n_{gr}}(a)\, \sigma_{\mathrm{gr}}(a)\, \mathrm{d}a \quad . \tag{A15}$$

$$= 2\pi k_1\, \mathrm{n_{gr}}(\mathrm{tot})\, \frac{a_{max}^{0.5} - a_{min}^{0.5}}{(a_{min} a_{max})^{0.5}} \quad , \tag{A16}$$

where equations (A11), (A5), and (A13) were used. The $\mathrm{n_{gr}}(\mathrm{tot})$ on the right side must now be expressed in terms of the molecular gas density, $\mathrm{n_{H2}}$. This can be done using an expression analogous to that of (A3) that uses the range of dust sizes:

$$\mathrm{n_{gr}}(\mathrm{tot})\langle\mathrm{m_{gr}}(a)\rangle_a = x_d \mathrm{n_{H2}} \mathrm{m_{H2}} \quad , \tag{A17}$$

or

$$\int_{a_{min}}^{a_{max}} n_{gr}(a)\, m_{gr}(a)\, da = x_d n_{H2} m_{H2} \quad .$$

Applying equations (A4), (A11), and (A13) yields

$$\frac{4\pi}{3}\rho_{gr} n_{gr}(tot)\, k_1 \int_{a_{min}}^{a_{max}} a^{-0.5} da = x_d n_{H2} m_{H2} \quad .$$

Integrating and solving for $n_{gr}(tot)$ gives us

$$n_{gr}(tot) = \frac{3\, x_d n_{H2} m_{H2}}{8\pi \rho_{gr} k_1 (a_{max}^{0.5} - a_{min}^{0.5})} \quad . \tag{A18}$$

Substituting (A18) into the right side of (A16) yields

$$n_{gr}(tot)\langle \sigma_{gr}(a) \rangle_a = \frac{3}{4}\frac{x_d n_{H2} m_{H2}}{a_{eff}\rho_{gr}} \quad , \tag{A19}$$

where

$$a_{eff} \equiv (a_{min} a_{max})^{0.5} \quad . \tag{A20}$$

Equation (A19) replaces the $n_{gr}\sigma_{gr}$ that appears in (A1), yielding an expression nearly identical to (A8) and (A9), except that a is replaced with a_{eff}. Therefore, the relevant grain radius in the expressions for Λ_{gd} (e.g., equation A9) is the geometric mean of the minimum and maximum grain sizes (i.e., equation A20).

The a_{min} and a_{max} should be those for the big grains, rather than for the full range of dust sizes that also include the VSGs (very small grains) and the PAHs (polycyclic aromatic hydrocarbons) (e.g., see Désert et al. 1990). The big grains are in thermal equilibrium and are the grains observed with the $140\,\mu$m and $240\,\mu$m *DIRBE* observations. According to Désert et al. (1990), the a_{min} and a_{max} are 15 and 110 nm, respectively, for the big grains. This gives $a_{eff} = 41$ nm and increases Λ_{gd} by a factor of 4.2. The full range of sizes over all grains, i.e. $a_{min} = 0.4$ nm and $a_{max} = 110$ nm, results in $a_{eff} = 6.6$ nm and Λ_{gd} is increased by a factor of 26. However, there are at least two problems with using the full size range of grains. One is that, as mentioned above, only the big grains are relevant to the observations discussed here. The second is that the treatment above implicitly assumes that, within the grain size distribution, only the grain size changes; other grain properties, such as grain density and shape, are assumed constant despite changing grain size. For example, going from (A17) to (A18) assumes that ρ_{gr} is independent of a. This is likely to be a bad approximation for the full size range, especially when grain type varies with grain size (e.g., see Désert et al. 1990). Therefore, the factor of 4.2 increase in Λ_{gd} is appropriate when only considering the big grains.

A few corrections should be considered before using that factor of 4.2. Given that only the big grains were used, we must correct for not using the full population of dust

grains. Specifically, the dust-to-gas mass ratio used must be replaced by the mass ratio of the dust in big grains to that of the gas. The grain densities and sizes in Désert et al. (1990) imply that the big grains represent 76% of the mass of the dust. However, a more appropriate accommodation factor is necessary for the low dust and gas temperatures that considered here. This suggests that $\bar{\alpha}_T$ is 0.4 instead of 0.3 (see Burke & Hollenbach 1983). Accordingly, increasing the accommodation factor while decreasing the dust-to-mass ratio by similar amounts gives an overall correction of nearly unity (in fact it is about 0.9). Another possible correction, or at least uncertainty, is the density adopted for the big grains. While Goldsmith (2001) adopts $\rho_{gr} = 2\,\mathrm{g\cdot cm^{-3}}$, Désert et al. (1990) use $3\,\mathrm{g\cdot cm^{-3}}$ for the big grains. This latter density brings the 4.2 factor down to about 3.

In conclusion, considering a realistic range of grain sizes increases the gas-grain thermal coupling by factors of about 3 to 4.

REFERENCES

Abbas, M. M., Craven, P. D., Spann, J. F., Tankosic, D., LeClair, A., Gallagher, D. L., West, E. A., Weingartner, J. C., Witherow, W. K., and Tielens, A. G. G. M. 2004, ApJ, 614, 781

Bally, J., Stark, A. A., Wilson, R. W., and Henkel, C. 1987, ApJS, 65, 13

Bally, J., Langer, W. D., and Liu, W. 1991, ApJ, 383, 645

Boreiko, R. T. and Betz, A. L. 1989, ApJ, 346, L97

Boulanger, F., Bronfman, L., Dame, T. M., and Thaddeus, P. 1998, A&A, 332, 273

Boulanger, F., Falgarone, E., Puget, J.-L., and Helou, G. 1990, ApJ, 369, 136

Burke, J. R. and Hollenbach, D. J. 1983, ApJ, 265, 223

Cernicharo, J., Pardo, J. R., Gonzlez-Alfonso, E., Serabyn, E., Phillips, T. G., Benford, D. J., and Mehringer, D. 1999, ApJ, 520, L131

COBE Diffuse Infrared Background Experiment (DIRBE) Explanatory Supplement 1998, version 2.3, ed. M. G. Hauser, T. Kelsall, D. Leisawitz, and J. Weiland, COBE Ref. Pub. 98-A (Greenbelt, MD: NASA/GSFC), available in electronic form from the NSSDC.

Cuillandre, J.-C., Lequeux, J., Allen, R. J., Mellier, Y., and Bertin, E. 2001, ApJ, 554, 190

Dame, T. M. 1993, Back to the Galaxy, AIP Conf. 278, ed. S. S. Holt and F. Verter, New York : AIP, 267

Davis, L., Jr. and Greenstein, J. L. 1951, ApJ, 114, 206

Désert, F.-X., Boulanger, F., & Puget, J. L. 1990, A&A, 237, 215

Dickman, R. L. 1975, ApJ, 202, 50

Dickman, R. L., Snell, R. L., and Schloerb, F. P. 1986, ApJ, 309, 326

Dupac, X., Giard, M., Bernard, J.-P., Lamarre, J.-M., Mény, C., Pajot, F., Ristorcelli, I., Serra, G., and Torre, J.-P. 2000, ApJ, 553, 604

Dwek, E. 2004, ApJ, 607, 848

Finkbeiner, D. P., Davis, M., and Schlegel, D. J. 1999, ApJ, 527, 867

Fixsen, D. J., Bennett, C. L., and Mather, J. C. 1999, ApJ, 526, 207

Goldsmith, P. F. 2001, ApJ, 557, 736

Goldsmith, P. F., Bergin, E. A., and Lis, D. C. 1997, ApJ, 491, 615

Graf, U. U., Eckart, A., Genzel, R., Harris, A. I., Poglitsch, A., Russell, A. P. G., and Stutzki, J. 1993, ApJ, 405, 249

Graf, U. U., Genzel, R., Harris, A. I., Hills, R. E., Russell, A. P. G., and Stutzki, J. 1990, ApJ, 358, L49

Güsten, R., Serabyn, E., Kasemann, C., Schinkel, A., Schneider, G., Schulz, A., and Young, K. 1993, ApJ, 402, 537

Hall, J. S. 1949, Science, 109, 166

Harris, A. I., Hills, R. E., Stutzki, J., Graf, U. U., Russell, A. P. G., and Genzel, R. 1991, ApJ, 382, L75

Harris, A. I., Jaffe, D. T., Silber, M., and Genzel, R. 1985, ApJ, 294, L93

Harrison, A., Henkel, C., and Russell, A. 1999, ApJ, 303, 157

Heiles, C., Haffner, L. M., Reynolds, R. J., and Tufte, S. L. 2000, ApJ, 536, 335

Heyer, M. H., Carpenter, J. M., and Ladd, E. F. 1996, ApJ, 463, 630

Hiltner, W. A. 1949, ApJ, 109, 471

Howe, J. E., Jaffe, D. T., Grossman, E. N., Wall, W. F., Mangum, J. G., and Stacey, G. J. 1993, ApJ, 410, 179

Johnstone, D. and Bally, J. 1999, ApJ, 510, L49

Jones, R. V. and Spitzer, L., Jr. 1967, ApJ, 147, 943

Lagache, G., Abergel, A., Boulanger, F., and Puget, J.-L. 1998, A&A, 333, 709

Lazarian, A., Goodman, A. A., and Myers, P. C. 1997, ApJ, 490, 273

Leisawitz, D. and Hauser, M. J. 1988, ApJ, 332, 954

Lis, D. C., Serabyn, E., Zylka, R., and Li, Y. 2001, ApJ, 550, 761

Mangum, J. G., Wootten, A., and Barsony, M. 1999, ApJ, 526, 845

Mao, R.Q., Henkel, C., Schulz, A., Zielinsky, M., Mauersberger, R., Störzer, H., Wilson, T.L., and Gensheimer, P. 2000, å, 358, 433

Mathis, J. S., Mezger, P. G., and Panagia, N. 1983 A&A, 128, 212

Mathis, J. S., Rumple, W., and Nordsieck, K. H. 1977, ApJ, 217, 425

Merluzzi, P., Bussoletti, E., Dall'Oglio, G., and Piccorillo, L. 1994, ApJ, 436, 286

Mezger, P. G., Sievers, A. W., Haslam, C. G. T., Kreysa, E., Lemke, R., Mauersberger, R., and Wilson, T. L. 1992, A&A, 256, 631

Mochizuki, K. and Nakagawa, T. 2000, ApJ535, 118

Nagahama, T., Mizuno, A., Ogawa, H., and Fukui, Y. 1998, AJ, 116, 336

Osterbrock, D. E. 1989, Astrophysics of Gaseous Nebulae, Mill Valley : University Science Books

Plume, R., Bensch, F., Howe, J. E., Ashby, M. L. N., Bergin, E. A., Chin, G., Erickson, N. R., Goldsmith, P. F., Harwit, M., Kleiner, S., Koch, D. G., Neufeld, D. A., Patten, B. M., Scheider, R., Snell, R. L., Stauffer, J. R., Tolls, V., Wang, Z., Winnewisser, G., Zhang, Y. F., Reynolds, K., Joyce, R., Tavoletti, C., Jack, G., Rodkey, C. J., and Melnick, G. J. 2000, ApJ, L133

Reach, W. T., Dwek, E., Fixsen, D. J., Hewagama, T., Mather, J. C., Shafer, R. A., Banday, A. J., Bennett, C. L., Cheng, E. S., Eplee, R. E., Jr., Leisawitz, D., Lubin, P. M., Read, S. M., Rosen, L. P., Shuman, F. G. D., Smoot, G. F., Sodroski, T. J., and Wright, E. L. 1995, ApJ, 451, 188

Reach, W. T., Wall, W. F., and Odegard, N. 1998, ApJ, 507, 507

Ristorcelli, I., Serra, G., Lamarre, J. M., Giard, M., Pajot, F., Bernard, J. P., Torre, J. P., De Luca, A., and Puget, J. L. 1998, ApJ, 496, 267

Sakamoto, S., Hayashi, M., Hasegawa, T., Handa, T., and Oka, T. 1994, ApJ, 425, 641

Sanders, D. B. 1993, Sky Surveys: Protostars to Protogalaxies, ed. B. T. Soifer, San Francisco : ASP 43, 65

Sanders, D. B., Scoville, N. Z., and Solomon, P. M. 1985, ApJ, 289, 373

Schloerb, F. P., Snell, R. L., and Schwartz, P. R. 1987, ApJ, 319, 426

Schnee, S., Bethell, T., Goodman, A. 2006, ApJ, 640, L47

Scoville, N. Z. and Good, J. C. 1989, ApJ339, 149

Sellgren, K., Luan, L., and Werner, M. W. 1990, ApJ, 359, 384

Sodroski, T. J., Bennett, C., Boggess, N., Dwek, E., Franz, B. A., Hauser, M. G., Kelsall, T., Moseley, S. H., Odegard, N., Silverberg, R. F., and Weiland, J. L. 1994, ApJ, 428, 638

Sodroski, T. J., Dwek, E., Hauser, M. G., and Kerr, F. J. 1989, ApJ, 336, 762

Spitzer, L., Jr. 1978, Physical Processes in the Interstellar Medium, New York: Wiley

Swartz, P. R., Snell, R. L., and Schloerb, F. P. 1989, ApJ, 336, 519

Tielens, A. G. G. M. and Hollenbach, D. 1985, ApJ, 291, 722

Tielens, A. G. G. M. and Hollenbach, D. 1985, ApJ, 291, 747

Wall, W. F. 2007, MNRAS, 375, 278 (see also astro-ph) (Paper I)

Wall, W. F. 2007a, MNRAS, accepted (see also astro-ph) (Paper II)

Wall, W. F. 2007b, MNRAS, submitted (see also astro-ph)

Wall, W. F., Jaffe, D. T., Israel, F. P., and Bash, F. N. 1991, ApJ, 380, 384

Wall, W. F., Reach, W. T., Hauser, M. G., Arendt, R. G., Weiland, J. L., Berriman, G. B., Bennett, C. L., Dwek, E., Leisawitz, D., Mitra, P. M., Odenwald, S. F., Sodroski, T. J., and Toller, G. N. 1996, ApJ, 456, 566 (W96)

Warin, S., Benayoun, J. J., and Viala, Y. P. 1996, A&A, 308, 535

Weiss, A., Neininger, N., Hüttemeister, S., and Klein, U. 2001, å, 365, 571

Werner, M. W., Gatley, I., Harper, D. A., Becklin, E. E., Loewenstein, R. F., Telesco, C. M., and Thronson, H. A. 1976, ApJ, 204, 420

Wild, W., Harris, A. I., Eckart, A., Genzel, R., Graf, U. U., Jackson, J. M., Russell, A. P. G., and Stutzki, J. 1992, A&A, 265, 447

Wilson, T. L., Muders, D., Kramer, C., and Henkel, C. 2001, ApJ, 557, 240

Wolfire, M. G., Hollenbach, D., and Tielens, A. G. G. M. 1989, ApJ, 344, 370

Wu, Y. and Evans, N. J. 1989, ApJ, 340, 307

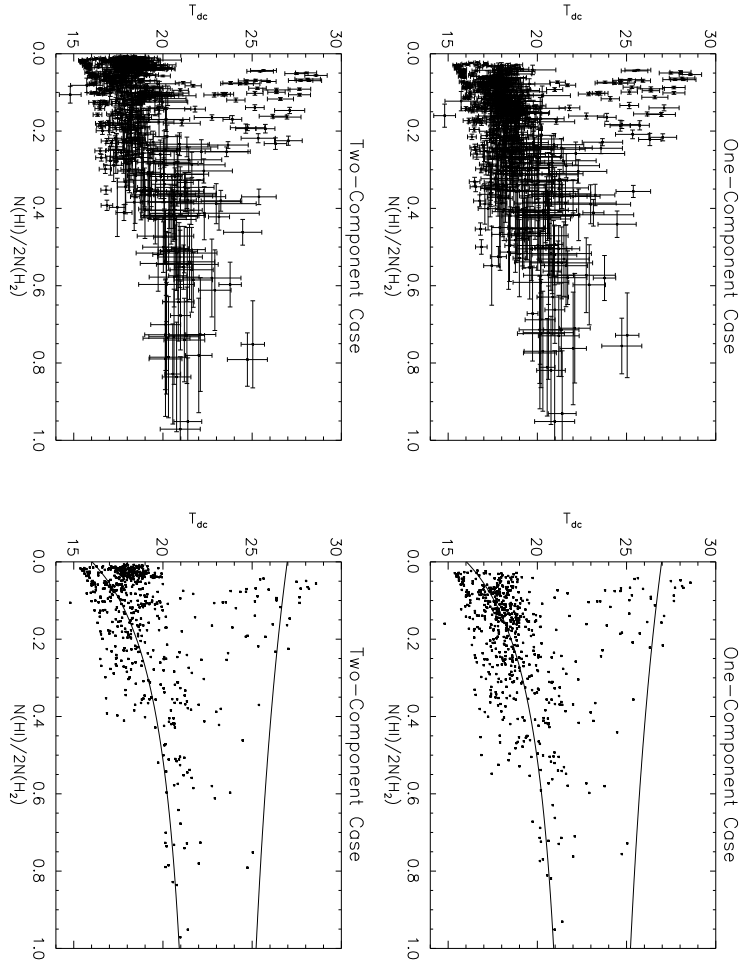Zhang, C. Y., Laureijs, R. J., Chlewicki, G., Clark, F. O., and Wesselius, P. R. 1989, A&A, 218, 231

Fig. 1.— Plots of the $140\,\mu$m/$240\,\mu$m dust color temperature versus the ratio of the atomic gas to molecular gas column densities, $N(H\,I)/2N(H_2)$, appear above. The upper two panels show these plots for the one-component, LVG models. The lower two panels are for the two-component, two-subsample, LVG models. The panels on the left include the error bars, while the panels on the right exclude the error bars. The curves in the panels on the right represent hypothetical cases where the dust associated with the molecular gas has one fixed temperature for all lines of sight and the dust associated with the atomic gas has another fixed temperature. The lower curve in each of the right panels assumes that the dust in the molecular gas has $T_d = 16.5\,$K and the dust in the atomic gas has $T_d = 22.5\,$K. The upper curve in each of the right panels assumes $T_d = 27\,$K and $22.5\,$K for the dust associated with molecular and atomic gas, respectively. The plots only include those pixels with the intensities above the 5-σ level in $I_\nu(140\,\mu$m$)$, $I_\nu(240\,\mu$m$)$, $I(^{13}$CO$)$ and above the 3-σ level in $I(H\,I)$ *simultaneously*.
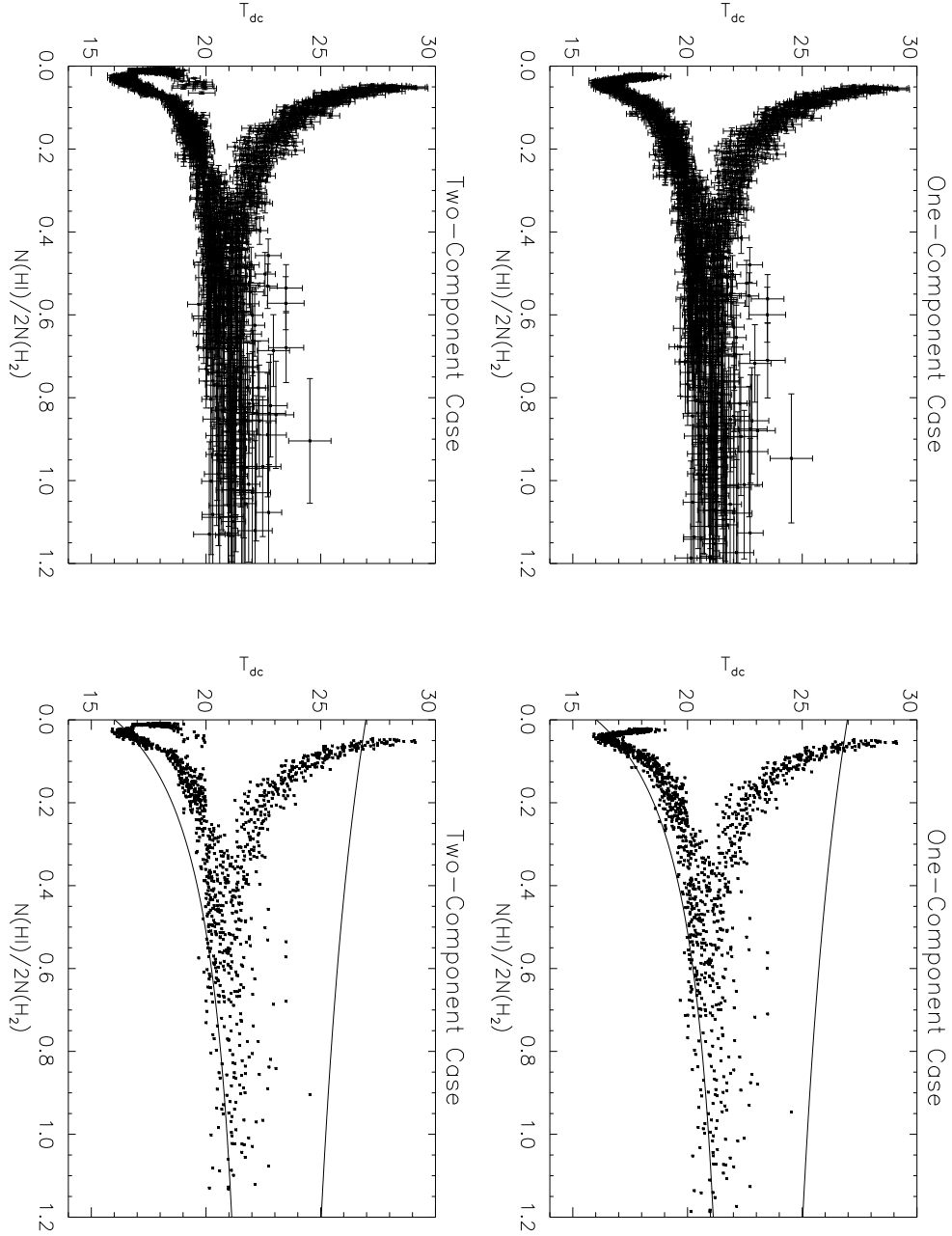
Fig. 2.— The is the equivalent of Figure 1, but for the *simulated* data. The H I layer has a constant column density of $5 \times 10^{20}\, H\; atoms \cdot \mathrm{cm}^{-2}$ and a constant dust temperature of $22.5\,\mathrm{K}$. The curves are the same as those in Figure 1.
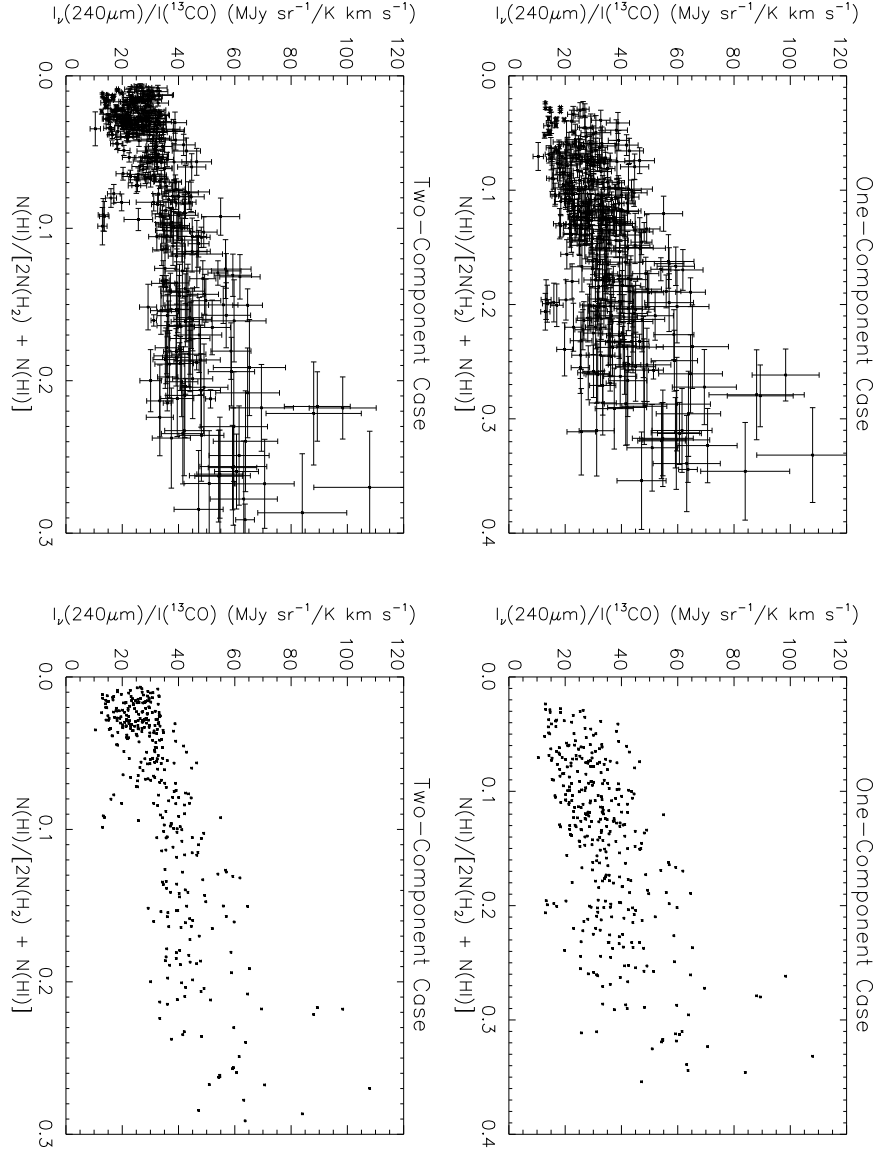
Fig. 3.— Plots of the $I_\nu(240\,\mu m)/I(^{13}CO)$ ratio versus the atomic hydrogen fraction, $N(H\,I)/[N(H\,I)+2N(H_2)]$ are shown for a subsample of the high signal-to-noise positions with a $140\,\mu m/240\,\mu m$ color temperature, T_{dc}, near $18\,K$. Specifically, this sample of points is higher than 5σ in $I_\nu(140\,\mu m)$, $I_\nu(240\,\mu m)$, and $I(^{13}CO)$, higher than 3σ in $I(H\,I\ 21\,cm)$, and with T_{dc} in the range 17 to $19.5\,K$. The upper plots use the $N(H_2)$ values of the non-LTE, one-component models and the lower plots use those of the non-LTE, two-component, two-subsample models. The left plots include the error bars and right plots omit the error bars for clarity.
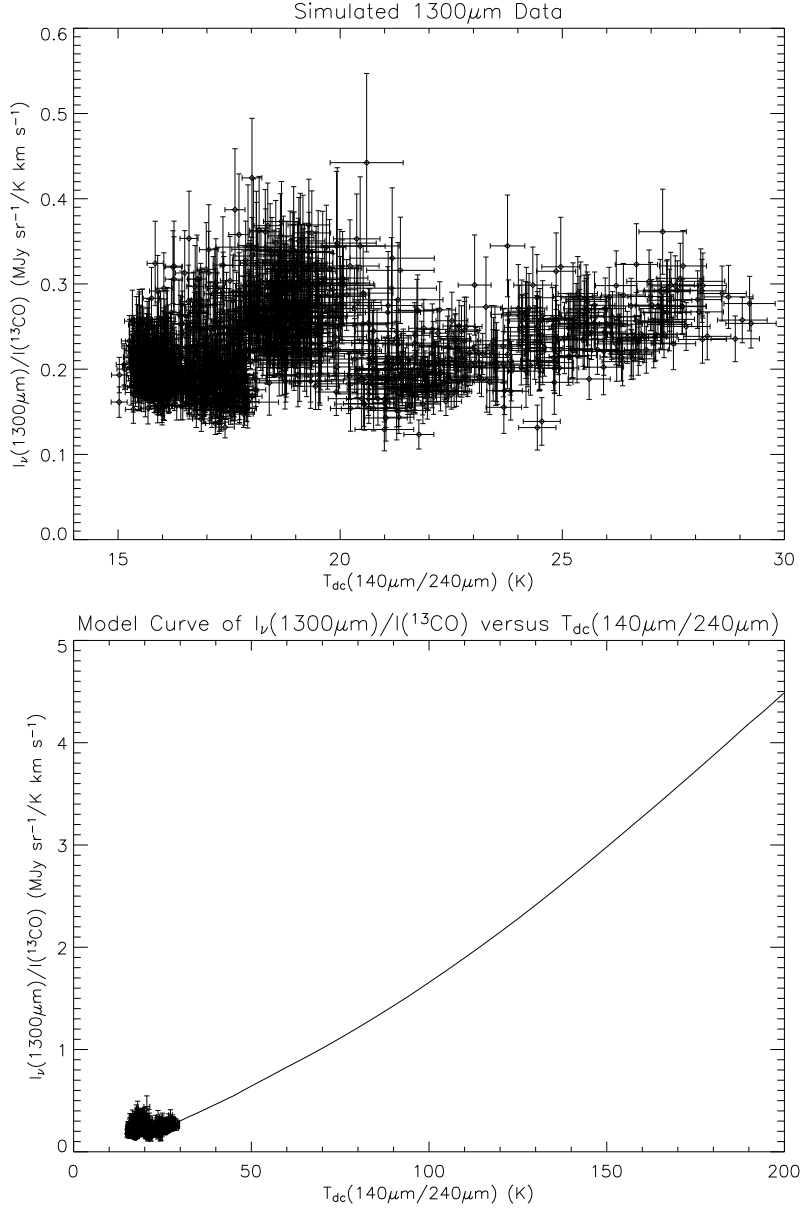
Fig. 4.— These are plots of simulated $1300\,\mu$m continuum to ^{13}CO J $= 1 \rightarrow 0$ spectral line ratio data, i.e. $I_\nu(1300\,\mu$m$)/I(^{13}$CO$)$, versus simulated $140\,\mu$m$/240\,\mu$m color temperature data, i.e. T_{dc}. The simulations use the parameters listed in the second column of Table 1 of Paper II and a mass absorption coefficient appropriate for $\lambda = 1300\,\mu$m (see details in Section 4.6). The upper panel is the plot of $I_\nu(1300\,\mu$m$)/I(^{13}$CO$)$ versus T_{dc} for the temperature range $T_{dc} = 14$ to 30 K. The lower panel plots the same quantities, but for the larger temperature range of $T_{dc} = 0$ to 200 K. The lower panel also shows the model curve out to $T_{dc} = 200$ K.

Table 1.   Best-Fit Parameter Values for the Different Models

One-Component Models

LTE
Full Sample

ΔT	χ^2_ν	ν
-4	16.5	673

$T_d > 20\,K$

9	9.0	140

LVG
Full Sample

ΔT	$\frac{N(^{13}CO)}{\Delta v}$	$n(H_2)$	χ^2_ν	ν
-1	3×10^{15}	1×10^5	16.9	671

$T_d > 20\,K$

-3	3×10^{15}	6×10^3	10.0	139

Two-Component Models

Full Sample

ΔT	c_0	T_{d0}	$\frac{N_{c0}(^{13}CO)}{\Delta v_c}$	n_{c0}	$\frac{N_{c1}(^{13}CO)}{\Delta v_c}$	n_{c1}	χ^2_ν	ν
0	0.04	18	5×10^{16}	2×10^4	8×10^{15}	1×10^3	5.7	667

Two Subsample
$T_d < 20\,K$

ΔT	c_0	T_{d0}	$\frac{N_{c0}(^{13}CO)}{\Delta v_c}$	n_{c0}	$\frac{N_{c1}(^{13}CO)}{\Delta v_c}$	n_{c1}	χ^2_ν	ν
0	1.0	18	5×10^{15}	1×10^5	2×10^{16}	1×10^5	4.6	525

$T_d > 20\,K$

0	0.4	18	5×10^{14}	1×10^4	5×10^{15}	6×10^3	8.2	135

Note. — ΔT and T_{d0} are in units of Kelvins. The $N(^{13}CO)/\Delta v$ quantities are in units of $^{13}CO\ molecules \cdot cm^{-2} \cdot (km \cdot s^{-1})^{-1}$. The n quantities are in units of $H_2\ molecules \cdot cm^{-3}$. All two-component models used the LVG code. See Paper I for discussion of the formal and systematic uncertainties.

Table 2.   Best Estimates of Parameter Value Ranges[a]

Parameter	Range of Values
$\Delta \mathrm{T}^{\mathrm{b}}$	-1 to $+2\,\mathrm{K}$
$\mathrm{T_{d0}}$	16 to $19\,\mathrm{K}^{\mathrm{c}}$
$c_0 \frac{\mathrm{N_{c0}(^{13}CO)}}{\Delta \mathrm{v_c}}$	2.0×10^{14} to $5.0 \times 10^{15}\ ^{13}CO\ \mathrm{cm}^{-2} \cdot (\mathrm{km \cdot s}^{-1})^{-1}$
n_{c0}	$\gtrsim 20\ H_2\ \mathrm{cm}^{-3}$
$\frac{\mathrm{N_{c1}(^{13}CO)}}{\Delta \mathrm{v_c}}\mathrm{d}$	3×10^{15} to $2 \times 10^{16}\ ^{13}CO\ \mathrm{cm}^{-2} \cdot (\mathrm{km \cdot s}^{-1})^{-1}$
n_{c1}	$\gtrsim few \times 10^3\ H_2\ \mathrm{cm}^{-3}$

[a]See Paper II for details.

[b]Assuming two-component models applied to *both* subsamples.

[c]See Section 3.6.

[d]For the two-component models applied to the two subsamples, the $\frac{\mathrm{N_{c1}(^{13}CO)}}{\Delta \mathrm{v_c}}$ value would be at the higher end of this range for the $\mathrm{T_{dc}} < 20\,\mathrm{K}$ subsample and at the lower end for the $\mathrm{T_{dc}} \geq 20\,\mathrm{K}$ subsample.